



Seasonal Transport Pathway and Sources of Carbonaceous Aerosols at an Urban Site of Eastern Himalaya

Akansha Rai^{1,2} · Sauryadeep Mukherjee³ · Nikki Choudhary^{1,2} · Abhinandan Ghosh³ · A. Chatterjee³ · T. K. Mandal¹ · S. K. Sharma^{1,2} · R. K. Kotnala¹

Received: 1 April 2021 / Revised: 19 May 2021 / Accepted: 24 May 2021 / Published online: 8 June 2021
© Institute of Earth Environment, Chinese Academy Sciences 2021

Abstract

In this study, we examined the seasonal transport pathways of carbonaceous species [Organic Carbon (OC), Elemental Carbon (EC), Water-Soluble Organic Carbon (WSOC), Primary Organic Carbon (POC), Secondary Organic Carbon (SOC), and Total Carbonaceous Aerosols (TCAs)] of PM_{2.5} and PM₁₀ over a semi-urban high-altitude site of Darjeeling (27.041°N, 88.266°E, 2200 m above mean sea level (amsl); an eastern Himalayan region), India during August 2018–July 2019. The annual average concentrations of PM_{2.5} and PM₁₀ were $37 \pm 12 \mu\text{g m}^{-3}$ and $55 \pm 18 \mu\text{g m}^{-3}$, respectively that was within but quite close to the threshold limit of National Ambient Air Quality Standards (NAAQS) (annual $60 \mu\text{g m}^{-3}$ for PM₁₀; and $40 \mu\text{g m}^{-3}$ for PM_{2.5}). The seasonal average concentration of OC in PM_{2.5} was highest in pre-monsoon ($4.2 \pm 1.7 \mu\text{g m}^{-3}$) > post-monsoon ($4.0 \pm 1.6 \mu\text{g m}^{-3}$) > winter ($3.3 \pm 1.5 \mu\text{g m}^{-3}$) > monsoon ($2.2 \pm 0.9 \mu\text{g m}^{-3}$) whereas OC in PM₁₀, in the order of highest in post-monsoon ($5.9 \pm 2.4 \mu\text{g m}^{-3}$) > winter ($5.4 \pm 2.0 \mu\text{g m}^{-3}$) > pre-monsoon ($5.2 \pm 2.1 \mu\text{g m}^{-3}$) > monsoon ($3.6 \pm 0.9 \mu\text{g m}^{-3}$). Similar seasonal variation in case of EC in both PM_{2.5} (winter $1.8 \pm 0.8 \mu\text{g m}^{-3}$; pre-monsoon $2.2 \pm 0.9 \mu\text{g m}^{-3}$; monsoon $1.2 \pm 0.4 \mu\text{g m}^{-3}$; post-monsoon $2.2 \pm 1.1 \mu\text{g m}^{-3}$) and PM₁₀ (winter $2.7 \pm 1.0 \mu\text{g m}^{-3}$; pre-monsoon $3.0 \pm 1.1 \mu\text{g m}^{-3}$; monsoon $1.2 \pm 0.4 \mu\text{g m}^{-3}$; post-monsoon $1.9 \pm 1.2 \mu\text{g m}^{-3}$) were observed during the study period. Based on different altitudes (100, 500, 1000 m), the seasonal backward trajectory and its concentration-weighted trajectory (CWT) analysis reveal the local, Indo-Gangetic Plain (IGP), the Thar desert, semi-arid, central highlands, Nepal, and the Bay of Bengal (BoB) as the common pollutant transporting regions to the observational site of Darjeeling. Also, its cluster analysis at 500 m above ground level (AGL) indicates that air mass originates mainly from 3 sides [western region, Thar desert (17.6%); north-western region, Nepal (45.1%); southern region, Bangladesh (37.3%)] during the study. Due to high tourist influx in pre-monsoon (peak tourist season), the maximum contribution of carbonaceous aerosols was mainly from the vehicular sources, coal combustion, transboundary pollutants, biomass burning in the IGP region, and the formation of secondary organic aerosols (SOA). Besides, active Terra and Aqua MODIS fire and thermal anomalies (≥ 80 per cent) indicated the maximum prevalence of fire spots during pre-monsoon across India (except the Thar desert) followed by post-monsoon (due to crop-residue burning) in Punjab and Haryana.

Keywords PM · Carbonaceous aerosols · Backward trajectory · Cluster analysis · CWT · Fire count

1 Introduction

Air pollution has been growing increasingly in many areas of the globe over the past few decades, with far-reaching and harmful effects on the atmosphere and human health (WHO 2016; Saikawa et al. 2019). Particular matter (PM) is one of the most significant contaminants with damaging effects on air chemistry (air quality and visibility), the health of human beings, snow-based albedo and precipitation, Earth's global climate-influential radiation budget (Ghosh et al. 2014; Bikina and Sarin 2019; Pant and Harrison, 2012). The effect of

✉ S. K. Sharma
sudhir.npl@nic.in; sudhiresir@gmail.com

¹ CSIR-National Physical Laboratory, Dr. K. S. Krishnan Road, New Delhi 110 012, India

² Academy of Scientific and Innovative Research (AcSIR), Ghaziabad 201 002, India

³ Centre for Astroparticle Physics and Space Sciences, Bose Institute, Darjeeling 734 102, India

airborne particulates is closely related to their size (Tiwari et al. 2017). Therefore, size-segregated PM studies have shown that they deposited mainly within the tracheobronchial airways (PM₁₀), alveolar region (PM_{2.5}) (Chen et al. 2019), and bloodstream (PM₁) (Falcon-Rodriguez et al. 2016), respectively. Several epidemiological studies concluded that the causal risk factors for many harmful human health effects (Pope and Dockery 2006; WHO 2016), including respiratory illnesses (Hanigan et al. 2021; Valavanidis et al. 2008; Kim et al. 2017), cardiopulmonary (Hanigan et al. 2021; Du et al. 2016; Peter et al. 2005; Silva et al. 2016) and carcinogenic effects (Callén et al. 2011; Kim et al. 2017; Masiol et al. 2017; Loomis et al. 2013) are due to particulate pollution.

Among the airborne particulates, the importance of investigating carbonaceous aerosols has recently gained widespread recognition (Sharma et al. 2015, 2017; Pintér et al. 2017; Hedge et al. 2020), as it contributes ~30–70 per cent of PM_{2.5} mass over urban and rural atmospheres (Ram et al. 2020; Dumka et al. 2019). Carbonaceous aerosols are classified into two types, based on their chemical and physical properties, i.e., organic carbon (OC) and elemental carbon (EC) (Kontul et al. 2020; Xu et al. 2015). EC is a light-absorbing component composed of graphite-like organic compounds and emitted directly from incomplete combustion of fossil fuels, biomass, coal, and bio-fuels derived from anthropogenic sources (Xu et al. 2015; Dinoi et al. 2017; Zhu et al. 2020; Zhang et al. 2020). When compared to greenhouse gases (GHGs), EC has a shorter atmospheric lifespan, ranging from a few days to weeks or hundreds of years. OC is the primary carbonaceous fraction (primary organic carbon, POC), emitted from the incomplete combustion of biomass and organic matter (Jafar and Harrison, 2020). OC is composed of various organic compounds, such as polycyclic aromatic hydrocarbons (PAHs), organic acids and alkanes, biphenyls that form secondary process through in situ reactions within the atmosphere (Arhami et al. 2018; Panicker et al. 2021; Srivastava and Naja 2020; Xu et al. 2015). EC has a positive radiative forcing effect in Earth-atmosphere system warming, while different compositions of OC can show different radiative forcing effect (i.e., negative as well as positive) that contributes to cooling and heating of the climate (Zhu et al. 2020; Babu et al. 2021; Aamaas et al. 2017). POC released from anthropogenic (cooking, traffic emissions, domestic heating, biomass and fossil fuel combustion) or biogenic sources (forest fires, vegetation, emissions from terpenes) (Dinoi et al. 2017; Kontul et al. 2020; Xu et al. 2015). Water-soluble organic carbon (WSOC) plays a substantial role in direct and indirect aerosol radiative forcing, hygroscopic properties, and serves as cloud condensation nuclei (CCN) (Panicker et al. 2021; Wei et al. 2019; Jin et al. 2020). WSOC can originate from

primary emissions or formed via a series of atmospheric oxidation of volatile organic compounds (VOCs) during transport and biogenic emissions (Jin et al. 2020; Wei et al. 2019). Previous studies (Jin et al. 2020; Rajput et al. 2013; Kirillova et al. 2013; Yu et al. 2014) have shown that biomass burning and secondary organic aerosol (SOA) are the two most significant sources of WSOC. Therefore, it is imperative to understand the chemical properties, temporal of carbonaceous aerosols, which may travel far from their origin because of their high atmospheric lifetime (several days to weeks) (Ram et al. 2020; Joshi 2020; Zhang 2020).

In the era of rapid climate change, aerosol pollution is a significant cause for the deterioration of extremely sensitive Himalayas and the surrounding areas (Hedge and Kawamura 2012; Sen et al. 2018; Ramachandran et al. 2020). Due to their complex topography and numerous glaciers, the Indian Himalayan Region (IHR) affects the Asian Monsoon and is influenced by global climate change (Yuan et al. 2020a). The eastern Himalayas stretches from eastern Nepal to Yunnan (China), across an area of 524,190 km² (Tse-ring et al. 2010). Anthropogenic activities such as cooking, open burning of agricultural residue and garbage, brick kilns, forest fires, motor vehicles, thermal power generation and other industries generate huge waste (Saikawa et al. 2019; Yuan et al. 2020a; Rai et al. 2020; Apollo et al. 2017). With the emission of carbonaceous particles, an essential trigger of glacial retreat in this fragile region may occur (Li et al. 2020a) and affect the health of a large populace of people, habitats, cryosphere, monsoon patterns, and agriculture (Saikawa et al. 2019; Ramachandran and Rupakheti 2021). A fourteen-month-long study of the carbonaceous aerosols fraction of ambient PM (PM₁₀ and PM_{2.5}) collected in Kangra (north-western Himalayan region) by Kumar and Attri (2015) concluded that the combustion of fuelwood which is a dominant source of carbonaceous aerosols (Sharma et al. 2021). During the land campaign in 2013, Sharma et al. (2014) reported the average concentrations of OC and EC of different locations of the north-western Himalayan region (Palampur, Kullu, Shimla, Solan, and Nahan) as $5.7 \pm 1.3 \mu\text{g m}^{-3}$ and $2.2 \pm 0.7 \mu\text{g m}^{-3}$ in PM_{2.5}. Trace gases mixing ratios and particulates concentrations vary spatially and reveal the potential impacts of local activities (Sharma et al. 2014).

Meteorological parameters including rainfall, wind speed, relative humidity (RH), wind direction, and temperature determine the dispersion and transport of airborne pollutants to local and distant regions and establish their temporal and spatial variability (Hernández-Ceballos et al. 2019). Due to their high atmospheric lifespan, carbonaceous aerosols can be transported from long distant source regions (7–10 days in the absence of precipitation) (Chatterjee et al. 2020). Air mass trajectory analysis is, therefore, a crucial scientific tool to determine the origin (local or regional) and transport of

pollutants (Chen et al. 2018; Ghosh et al. 2015; Hernández-Ceballos et al. 2019).

Air quality in the Himalayas, due to its high altitude, has a profound effect in terms of climate change and biogeochemical cycles, as it transports different types of pollutants over longer distances, resulting in alter air quality of the region (Joshi et al. 2020; Sharma et al. 2021; Saikawa et al. 2019). Because of its proximity to the altitudinal gradient, glaciers, topography, and rich bio-diversity, the carbonaceous aerosols are extremely important in the eastern Himalayan region (Lamsal et al. 2017; Sharma et al. 2020, 2021). It is, therefore, essential to investigate the ground-based aerosol measurements and understand the seasonal changes of both fine and coarse particulates over the eastern Himalayan region (Zhang et al. 2018; Sharma et al. 2021; Joshi et al. 2020). With that in mind, this paper aims to identify and estimate the probable pollutant areas over the eastern Himalayan region. The main goal of this study is to monitor the annual and seasonal variations of carbonaceous aerosols in PM_{10} and $PM_{2.5}$ at a high-altitude location (Darjeeling). To determine their possible source region of emissions, we used CWT analysis coupled with long-term data on ambient air quality, which is a useful tool for identifying local and regional sources.

2 Methodology

2.1 Study Site Description

The aerosol study was investigated in Indian Himalayan city, i.e., Darjeeling ($27.041^{\circ}N$, $88.266^{\circ}E$, ~ 2200 m amsl) (Fig. 1). Geographically, Darjeeling is adjacent to the Indo-Gangetic Plain (IGP), which is a global hotspot for high aerosol loads and is among the few areas of the planet that have endured enhancements (Ojha et al. 2020). Darjeeling is internationally renowned as a tourist destination for its spectacular view of Mt. Kanchenjunga (world's third highest mountain), along with its tea industry and the Darjeeling Himalayan Railway ("Toy Train"), which a UNESCO World Heritage site. Nevertheless, Darjeeling is most vulnerable to Sikkim, East Nepal, and West Bhutan among the administrative units (Bhattacharaya et al. 2020). The monitoring site is situated within the Bose Institute campus ($27.01^{\circ}N$, $88.15^{\circ}E$, ~ 2200 m AMSL) located 200 m away from the main town. Mixed emission sources such as local motor vehicle emissions, wood and biomass burning, waste burning, ammonia fertilizer farming practices, coal combustion (from the 'Toy Train'), and transport pollutants influenced the sampling site (Chatterjee et al. 2010; Sharma et al. 2020, 2021; Bhattacharya et al. 2020).

The Indian Meteorological Department (IMD) reports that the year should be classified as four distinct seasons,



Fig. 1 Sampling site in Darjeeling (Source: Google map)

i.e., winter (January–February), pre-monsoon (March, April, May), monsoon (June, July, August, September), and post-monsoon season (October, November, December). With heavy monsoon precipitation and cold in winter, the complex labyrinthine mountains with bold spurs, ridges, and valleys greatly vary their weather. The two-tourist season highlights of Darjeeling are pre-monsoon and post-monsoon (Chatterjee et al. 2010; 2020). Meteorological parameters were also recorded continuously during the sampling period using an automated weather station (AWS) installed at the sampling site. Darjeeling is considered a subtropical and temperate climate with wet summers because of heavy rain in the monsoon season. The annual minimum and maximum temperatures are $3.4^{\circ}C$ and $12.2^{\circ}C$ with the monthly average temperature ranging from 5.8 to $17.2^{\circ}C$. The average rainfall in the monsoon season was 3092 mm (on average, 126 rainy days per year). The monthly average temperature, RH, wind directions, and wind speed during the study period are summarized in Fig. 2. The detailed information about the study site is available in our previous publications and reference therein (Sharma et al. 2020; Rai et al. 2020; Ghosh et al. 2020; Chatterjee et al. 2020).

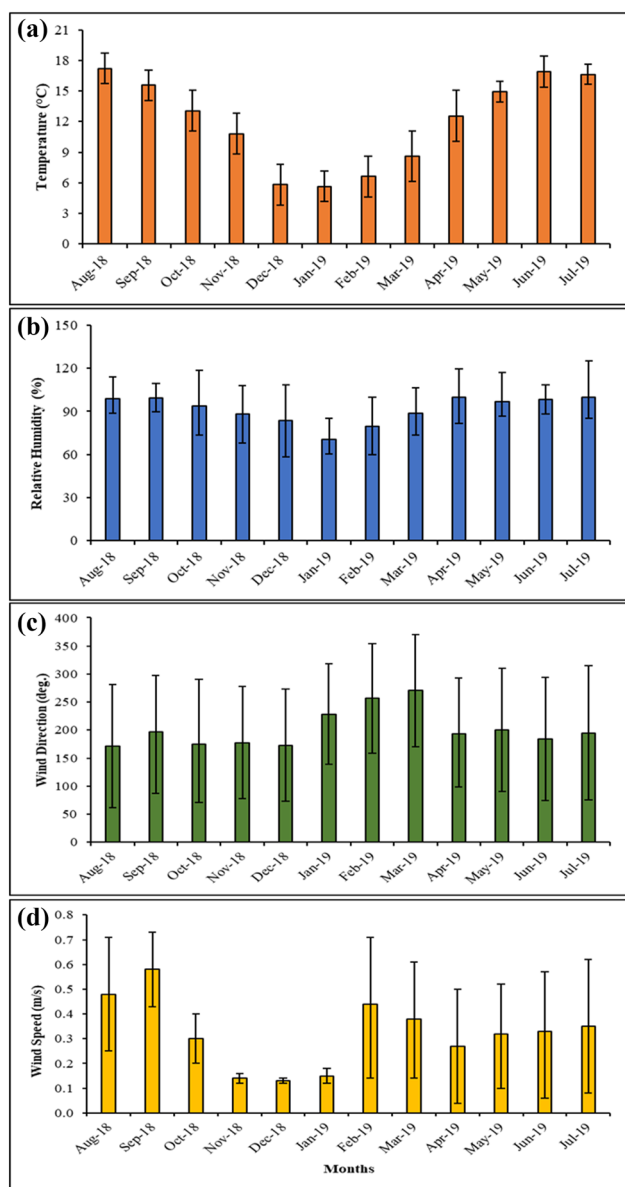


Fig. 2 Monthly average (a) temperature, (b) relative humidity (RH), (c) wind direction, and (d) wind speed during 2018–2019 at Darjeeling

2.2 Sample Collection

The ($PM_{2.5}$ and PM_{10}) sampling system is installed at the rooftop of Bose Institute's building at an altitude of 15 m above the ground level (AGL). $PM_{2.5}$ ($n=94$) and PM_{10} ($n=99$) samples were collected from August 2018 to July 2019 ($PM_{2.5}$ sampling was carried out up to June 2019 only). A fine particulate sampler (Envirotech Instrument Pvt. Ltd, India) and respirable particle sampler (Envirotech Instrument Pvt Ltd, India) were used to collect the $PM_{2.5}$ and PM_{10} samples, respectively. Through PALLFLEX quartz micro-fiber filters (M/s. PallFlex Products Co, USA), ambient air

was passed at an average flow rate of $1 \text{ m}^3 \text{ h}^{-1}$ for $PM_{2.5}$ and $\sim 1.2 \text{ m}^3 \text{ min}^{-1}$ for PM_{10} with an accuracy of $\pm 2\%$ for 24 h. Filters having a size of 47 mm for $PM_{2.5}$ and $20 \times 25 \text{ cm}^2$ for PM_{10} were pre-baked at $550 \text{ }^\circ\text{C}$ for no less than 5 h, before their use to remove contaminants present in the filter material. Filters were accurately weighed using a microbalance (M/s. Sartorius, resolution: $\pm 10 \text{ } \mu\text{g}$) before and after sampling to obtain the mass difference between the initial and final weight. Aerosol mass concentrations ($\mu\text{g m}^{-3}$) were estimated by PM mass difference (in μg) to the total volume of air (m^3) passed during the sampling period. The loaded filters were carefully placed in sealed bags (for PM_{10}) and cassettes (for $PM_{2.5}$) and stored in a deep freezer ($-20 \text{ }^\circ\text{C}$) until or chemical analysis.

2.3 Chemical Analysis

2.3.1 OC and EC Analysis

An OC/EC carbon analyzer (Model: DRI 2001A, Atmospheric Inc., Calabasas, CA, USA) was used to determine the concentration of OC and EC in PM that follows USEPA Method (IMPROVE carbon protocol). It works on thermal-optical method based on the preferential oxidation of both OC ($\text{OC} = \text{OC1} + \text{OC2} + \text{OC3} + \text{OC4} + \text{OP}$) in pure helium and EC ($\text{EC} = \text{EC1} + \text{EC2} + \text{EC3} - \text{OP}$) in 98% helium and 2% oxygen at elevated temperatures of $140 \text{ }^\circ\text{C}$, $280 \text{ }^\circ\text{C}$, $480 \text{ }^\circ\text{C}$ and $580 \text{ }^\circ\text{C}$ for OC fractions, and $580 \text{ }^\circ\text{C}$, $740 \text{ }^\circ\text{C}$ and $840 \text{ }^\circ\text{C}$ for EC fractions along with pyrolyzed carbon fraction (OP) (Chow et al. 2004). Its main goal is to check the pyrolysis and carbonization of OC compounds into EC, i.e., laser reflection, and the analyzer's transmission. Along with field blank filters, a known punch area of 0.536 cm^2 of the filter was cut and analyzed in triplicate with 3–5% analytical error (repeatability). The calculated OC and EC values for blank filters were subtracted from the obtained value of sample filters to estimate the correct OC and EC concentrations. There is a detailed overview of the analytical methods and calibration process and reference therein (Sharma et al. 2014; 2020; Rai et al. 2020).

2.3.2 WSOC Analysis

The known punch sizes of $PM_{2.5}$ ($\sim 3.46 \text{ cm}^2$) and PM_{10} ($\sim 7.07 \text{ cm}^2$) were cut into four halves and soaked in 20 ml of deionized water (resistivity $18.2 \text{ M}\Omega\text{-cm}$) and ultrasonicated three times for 10 min each. After filtration, the purified extract was diluted and analyzed for WSOC using a TOC analyzer (Model: Shimadzu TOC-L CPH/CPN, Japan). It works on the principle of catalytically aided combustion oxidation with a temperature of $680 \text{ }^\circ\text{C}$ that transforms the carbon components into CO_2 which is detected by a non-dispersive infrared (NDIR) gas analyzer. The measured total carbon (TC) and

inorganic carbon (IC) values for blank filters were subtracted from the sample filters to estimate the correct WSOC concentrations, which is calculated by the difference between TC and IC measurements. Based on each filter's triplicate analysis, the WSOC analytical error (repeatability) was calculated to be 3–10%. Details of the analytical methods and calibration process are given in Rai et al. (2020).

2.4 Estimation of TCA, POC and SOC

To account for the unmeasured H, O, N, and S in organic compounds, a conversion factor (or multiplier) is used to transform OC to OM ($OM = f \times OC$). The f multipliers of 1.4 and 1.8 are depending on the extent of OM oxidation and secondary organic aerosols (SOA) formation, values for f vary from 1.2 for fresh aerosol in urban areas (Chow et al. 2002) to 2.6 for aged aerosol (Robinson et al. 2010). In the present case, the total carbonaceous aerosols (TCAs) were calculated by the proposed method of Srinivas and Sarin (2014), that is the sum of EC and organic matter ($OM = 1.6 \times OC$) of PM_{10} (the 1.6 factor is used for PM_{10} ; whereas, for $PM_{2.5}$, 1.4 was used (Chow et al., 2004; Robinson et al. 2010)). According to Zhang et al. (2005), a conversion factor of $OC > 1.4$ for sub-urban aerosols was used. We assumed 1.6 as a factor to convert OC to OM because the sampling location is a desirable sub-urban location (Sharma et al. 2018; Rai et al. 2020).

According to Castro et al. (1999), primary organic carbon (POC) is calculated using the EC tracer approach by considering a minimum OC/EC ratio for each season [(winter 1.40 for $PM_{2.5}$ and 1.31 for PM_{10}), summer 1.22 for $PM_{2.5}$ and 1.27 for PM_{10}), monsoon 1.30 for $PM_{2.5}$ and 1.62 for PM_{10}) and post-monsoon 1.05 for $PM_{2.5}$ and 1.50 for PM_{10}]. EC and POC are known to derive from combustion sources, and EC is considered as a robust tracer for POC. The following relation is used to determine POC or OC_{primary} :

$$OC_{\text{primary}} = [OC/EC]_{\text{min}} \times [EC] + c, \quad (1)$$

where $(OC/EC)_{\text{min}}$ is the minimum ratio of OC/EC (minimum OC/EC for each season). c denotes the contribution from non-combustion sources, which in this case is negligible. Furthermore, for the estimation of secondary organic carbon (SOC or $OC_{\text{secondary}}$), the difference between the measured OC and estimated POC concentrations was calculated (Eq. 2).

$$OC_{\text{secondary}} = OC - OC_{\text{primary}}. \quad (2)$$

2.5 Backward Trajectory Analysis

Trajectory simulation techniques provide an effective and empirical way to classify areas associated with transporting

pollutants to specific geographic regions (NESCAUM 2002). In this type of analysis, the basic methodological approach is to produce enormous amounts of air mass trajectories to consider a large number of transport and dispersion scenarios, such that statistical analysis derives representative information about flow patterns (residence time, range, distance, speed, etc.) (Hernández-Ceballos et al. 2019).

We used the HYbrid-Single-Particle Lagrangian Integrated Trajectory (HYSPLIT) model (<https://www.ready.noaa.gov/HYSPLIT.php>) developed by the US National Oceanic and Atmospheric Administration's (NOAA) to explore the transport and circulation patterns of air pollutants that influence local and regional wind regimes. The Web-based HYSPLIT uses the $1^\circ \times 1^\circ$ GDAS (Global Data Assimilation System) meteorological data at the hour of 0500 UTC to simulate 3 days (72 h) backward trajectories (for each sampling day) using isentropic vertical velocity that is less susceptible to the uncertainties in the raw meteorological data due to the adiabatic vertical movements of air parcels enroute (Adak et al. 2013). The relative importance of long-distance versus regional emission sources was discerned by studying the different heights (100 m, 500 m, and 1000 m) analyzed (Ghosh et al. 2015). Trajectories are subject to interference from surface features (terrain and buildings) at lower altitudes, whereas higher-altitude trajectories may often be above the mixed layer and not reflect the air mass in the mixed layer (NESCAUM 2002).

MeteoInfo map is an application for a geographical information system that examines and visualizes various meteorological data formats (Li et al. 2020b). One of its plug-ins is TrajStat software that uses the HYSPLIT's trajectory to identify better potential sources and transport of pollutants over the specific region. Apart from trajectory analysis (backwards or forward), it also offers cluster, potential source contribution function (PSCF), and concentrated-weighted trajectory (CWT) analysis.

2.5.1 Cluster Analysis

Cluster analysis is a multivariate statistical technique that uses the Ward hierarchical method to outline the various airflows in the area (Xin et al. 2016; Markou and Kassomenos 2010; Zhang et al., 2018). The Ward's method (Eq. 3) based on the Euclidean distance is used to describe the latitude and longitude as distance variables between two trajectories, as shown in the following equation (Xin et al. 2016; Chen et al. 2018; Wang et al. 2009):

$$d_{ij} = \sqrt{\sum_{k=1}^p ((X_i(k) - X_j(k))^2 + (Y_i(k) - Y_j(k))^2)}, \quad (3)$$

where a point in p -dimensional space defines p , if the corresponding p -dimensional points are near, two observations are close to each other.

X_i and Y_i referred to the position of backward trajectory 1, and X_j and Y_j to the position of backward trajectory 2, respectively.

The ‘eyeball’ approach was used to calculate the required cluster number by comparing the mean trajectory figures (Chen et al. 2018). The number of clusters can be reduced by merging groups whose average trajectories are closest and retaining only those clusters that are noticeably different in wind speeds and wind direction. This approach’s main disadvantage is that if two back-trajectories have the same motion path but different speeds, they would be divided into two distinct categories (Xin et al. 2016).

2.5.2 Concentrated-Weighted Trajectory (CWT) Analysis

With simple trajectory analysis, aerosol particle pollution levels being transported to the receptor site cannot be extracted (Mahapatra et al. 2018; Zhu et al. 2018). In this regard, for source and receptor identification, CWT is an efficient trajectory-based receptor model that combines meteorological trajectory nodes (residence time) and pollutant concentrations to measure their pollution contribution to a receptor site (Suzuki et al. 2020; Li et al. 2020b). In the CWT algorithm (Eq. 4), the whole geographic region enclosed by trajectories divided into a grid area with longitude–latitude of (20.00, 70.00) in the northwest, (20.00, 10.00) in the southwest, (100.00, 70.00) in the north-east, and (100.00, 10.00) in the south-east; thus 19,200 grid cells were created. A weighted concentration is allocated to each grid cell ($0.5^\circ \times 0.5^\circ$ grid resolution) with the mean pollutant concentrations that cross the grid cell through corresponding trajectories (Zhao et al. 2018; Suzuki et al. 2020), as follows:

$$C_{ij} = \frac{1}{\sum_{k=1}^N \tau_{ijk}} \sum_{k=1}^N C_k \tau_{ijk}, \quad (4)$$

where C_{ij} is the average weighted concentration in the grid cell, (i, j)th. k : index of the trajectory, N : number of trajectories, C_k : pollutant concentrations measured at sampling location on import of trajectory k , and. τ_{ijk} : residence time (time spent) of the trajectory k in the grid cell (i, j)th.

2.5.3 Active Fire Data

To obtain the active fire spots over the Eastern Himalayan region during the sampling period, a contextual algorithm that targets the heavy emission from fires of mid-infrared radiation was used with a significant input of brightness temperature (4 μm and 11 μm channels). A particular type of MODIS (Moderate Resolution Imaging Spectroradiometer)

Collection 6 data (a combined product from Terra and Aqua, MCD14ML) from Fire Information for Resource Management System (FIRMS) was used. The improved algorithm of MODIS Collection 6 offers high efficiency in detecting small fires, enhanced cloud masking, reduction in a false alarm, and improved sunlight rejection with the best available active fire products. Using open-source GIS software *MeteoInfo*, data with a high confidence level ($> 80\%$) were collected and plotted. For more details, see MODIS Set 6 Active Fire Product User’s Guide Revision B.

3 Results and Discussion

3.1 Variation in Carbonaceous Components in $\text{PM}_{2.5}$ and PM_{10}

The annual average concentrations of $\text{PM}_{2.5}$ and PM_{10} were $37 \pm 12 \mu\text{g m}^{-3}$ (range 16–77 $\mu\text{g m}^{-3}$) and $55 \pm 18 \mu\text{g m}^{-3}$ (range 21–116 $\mu\text{g m}^{-3}$), respectively, that was quite close to the National Ambient Air Quality Standards (NAAQS) of India (annual limit 40 $\mu\text{g m}^{-3}$ for $\text{PM}_{2.5}$ and 60 $\mu\text{g m}^{-3}$ for PM_{10}) (Table 1). The maximum monthly average concentration of $\text{PM}_{2.5}$ was recorded in October (51 $\mu\text{g m}^{-3}$) and the minimum monthly average in January and June 2019 (27 $\mu\text{g m}^{-3}$). Similarly, the highest monthly average concentration of PM_{10} was recorded in March (73 $\mu\text{g m}^{-3}$), whereas the minimum monthly average concentration of PM_{10} was observed in December 2018 (39 $\mu\text{g m}^{-3}$). The monthly average mass concentrations of $\text{PM}_{2.5}$ and PM_{10} are depicted in Fig. 3; whereas, the monthly variation in mass concentrations of carbonaceous species of $\text{PM}_{2.5}$ and PM_{10} are shown in Fig. 4a, b, respectively. Overall, August 2018 depicts the minimum concentration of OC (in PM_{10} : 3.31 $\mu\text{g m}^{-3}$; in $\text{PM}_{2.5}$: 2.03 $\mu\text{g m}^{-3}$), EC (in PM_{10} : 0.82 $\mu\text{g m}^{-3}$; in $\text{PM}_{2.5}$: 0.98 $\mu\text{g m}^{-3}$), WSOC (in PM_{10} : 2.75 $\mu\text{g m}^{-3}$; in $\text{PM}_{2.5}$: 1.08 $\mu\text{g m}^{-3}$), POC (in PM_{10} : 2.73 $\mu\text{g m}^{-3}$; in $\text{PM}_{2.5}$: 1.67 $\mu\text{g m}^{-3}$), SOC (in PM_{10} : 0.58 $\mu\text{g m}^{-3}$; in $\text{PM}_{2.5}$: 0.36 $\mu\text{g m}^{-3}$) and TCAs (in PM_{10} : 6.11 $\mu\text{g m}^{-3}$; in $\text{PM}_{2.5}$: 3.82 $\mu\text{g m}^{-3}$) for both PM_{10} and $\text{PM}_{2.5}$. On the other hand, the maximum concentration of carbonaceous species of PM was observed in November 2018 and March 2019 for PM_{10} and $\text{PM}_{2.5}$, respectively. Except for EC (March 2019 for PM_{10} : 3.59 $\mu\text{g m}^{-3}$), POC (December 2018 for $\text{PM}_{2.5}$: 3.51 $\mu\text{g m}^{-3}$), and SOC (October 2018 for PM_{10} : 2.05 $\mu\text{g m}^{-3}$) which differ from other species. From the observed results, August 2018 was less polluted, whereas November 2018 and March 2019 were the most polluted months during the entire study period. Low carbonaceous concentration in August 2018 viz., the monsoon month is due to heavy rainfalls that wash off the pollutants. And the high carbonaceous concentration was observed in November

Table 1 Annual as well as seasonal average concentrations of PM_{2.5} and PM₁₀ and their chemical components (OC, EC, WSOC, TCAs, POC, and SOC) ($\mu\text{g m}^{-3}$) in Darjeeling

Species	Annual		Winter		Pre-monsoon		Monsoon		Post-monsoon	
	PM _{2.5} (n = 94)	PM ₁₀ (n = 102)	PM _{2.5} (n = 25)	PM ₁₀ (n = 25)	PM _{2.5} (n = 28)	PM ₁₀ (n = 32)	PM _{2.5} (n = 16)	PM ₁₀ (n = 20)	PM _{2.5} (n = 25)	PM ₁₀ (n = 25)
PM	37 ± 12	55 ± 18	30 ± 10	51 ± 18	41 ± 14	63 ± 21	38 ± 8	52 ± 12	40 ± 11	56 ± 16
OC	3.6 ± 1.6	5.1 ± 2.0	3.3 ± 1.4	5.4 ± 2.0	4.2 ± 1.7	5.2 ± 2.1	2.2 ± 0.9	3.6 ± 0.9	4.0 ± 1.6	5.9 ± 2.4
EC	1.9 ± 0.9	2.3 ± 1.2	1.8 ± 0.8	2.7 ± 1.0	2.2 ± 0.9	3.0 ± 1.1	1.2 ± 0.4	1.2 ± 0.4	2.2 ± 1.1	1.9 ± 1.2
WSOC	1.9 ± 1.0	3.6 ± 1.8	1.7 ± 1.0	3.9 ± 1.3	2.2 ± 1.2	3.4 ± 2.2	1.1 ± 0.5	2.3 ± 0.8	2.2 ± 1.0	4.8 ± 1.7
POC	2.0 ± 1.0	3.0 ± 1.5	2.5 ± 1.1	3.6 ± 1.3	2.7 ± 1.1	3.8 ± 1.5	1.6 ± 0.6	1.9 ± 0.6	2.3 ± 1.1	2.9 ± 1.8
SOC	1.5 ± 0.8	2.1 ± 1.2	0.8 ± 0.5	1.9 ± 1.1	1.4 ± 0.8	1.4 ± 1.0	0.6 ± 0.5	1.7 ± 0.9	1.7 ± 0.7	3.0 ± 1.0
TCAs	6.9 ± 3.1	10.4 ± 4.3	6.4 ± 2.7	11.4 ± 4.1	8.1 ± 3.2	11.3 ± 4.5	4.3 ± 1.6	6.9 ± 1.6	7.8 ± 3.2	11.4 ± 5.0

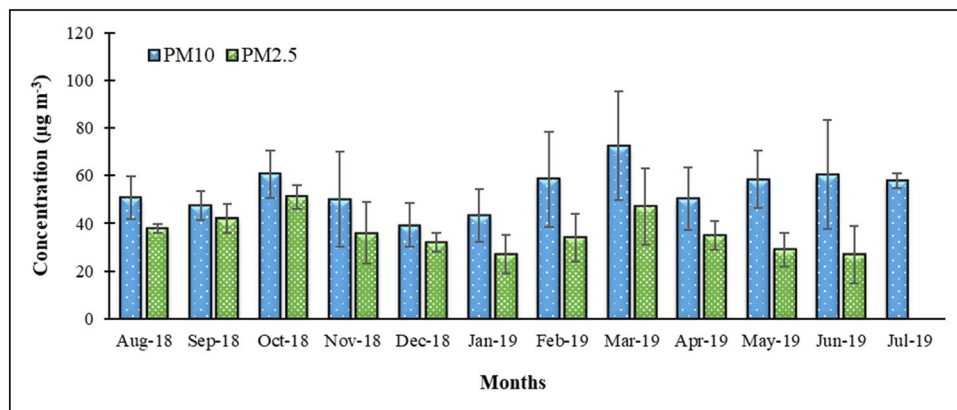
± Standard Deviation (at 1σ)

2018 (post-monsoon month) and March 2019 (pre-monsoon month), which are the peak tourist seasons in Darjeeling.

The average ratios of PM_{2.5}/PM₁₀ ranged from 0.59 to 0.72, indicating that over 68% of PM₁₀ in total is in the form of PM_{2.5}. In the present case, the highest seasonal average concentrations of both PM_{2.5} ($41 \pm 14 \mu\text{g m}^{-3}$) and PM₁₀ ($63 \pm 21 \mu\text{g m}^{-3}$) were recorded during the pre-monsoon season, followed by post-monsoon [PM_{2.5} ($40 \pm 11 \mu\text{g m}^{-3}$) and PM₁₀ ($56 \pm 16 \mu\text{g m}^{-3}$)] that might be because of the high influx of tourists in these seasons. Also, after the post-monsoon season, winter ($51 \pm 18 \mu\text{g m}^{-3}$) and monsoon ($52 \pm 12 \mu\text{g m}^{-3}$) concentrations were equivalent to each other (for PM₁₀); whereas, for PM_{2.5}, monsoon ($38 \pm 8 \mu\text{g m}^{-3}$) concentration was higher than winter ($30 \pm 10 \mu\text{g m}^{-3}$) (Table 1). The average concentration of carbonaceous species during winter, pre-monsoon, monsoon, and post-monsoon is shown in Fig. 5. For PM_{2.5}, the highest carbonaceous (OC, EC, WSOC, POC, TCAs) concentration was observed in pre-monsoon except for SOC concentration in post-monsoon that depicts more influence of tourism activities (Gajananda et al. 2005; Chatterjee et al. 2021) as well as long-range transportation of pollutants at sampling site of the Darjeeling (Rai et al. 2020). Whereas, lowest carbonaceous (OC, EC, WSOC, POC, SOC, TCAs) concentration was observed in monsoon, showing wash-out of pollutant loadings. Similarly, for PM₁₀, the lowest carbonaceous (OC, EC, WSOC, POC, TCAs) concentration was observed in monsoon except for SOC concentration in pre-monsoon; whereas, the highest carbonaceous concentration was observed in pre-monsoon and post-monsoon due to the peak tourist seasons of Darjeeling. Therefore, emissions from vehicles, coal combustion, cooking, etc. lead to elevation of EC and POC concentrations in pre-monsoon; whereas, crop-residue burning, biomass burning and formation of SOA contribute to higher concentrations (OC, WSOC, SOC, TCAs) in post-monsoon.

The relation between atmospheric concentrations of OC and EC offers qualitative knowledge about the sources of carbonaceous species in PM. It is noted that if OC and EC are both released into the atmosphere by the same primary source, the two carbonaceous species should be closely related (Dinoi et al. 2017; Sharma et al. 2020; Rai et al. 2020). The scatter plots of OC versus EC concentrations, in both size fractions, during winter, pre-monsoon, monsoon, and post-monsoon are given in Fig. S3 (in supplementary information) for Darjeeling. The solid lines indicate the linear regressions of data. Good correlations were found in winter ($R^2 = 0.77$, $R^2 = 0.88$ with $p < 0.05$), pre-monsoon ($R^2 = 0.85$, $R^2 = 0.87$ with $p < 0.05$), and post-monsoon ($R^2 = 0.74$, $R^2 = 0.80$ with $p < 0.05$); whereas, weaker correlation is found in monsoon ($R^2 = 0.09$, $R^2 = 0.63$ with $p < 0.05$) in PM₁₀ and PM_{2.5}, respectively, suggesting their common sources (Sharma et al. 2014; Ram and Sarin 2010).

Fig. 3 Monthly average concentrations of PM_{2.5} and PM₁₀ over Darjeeling



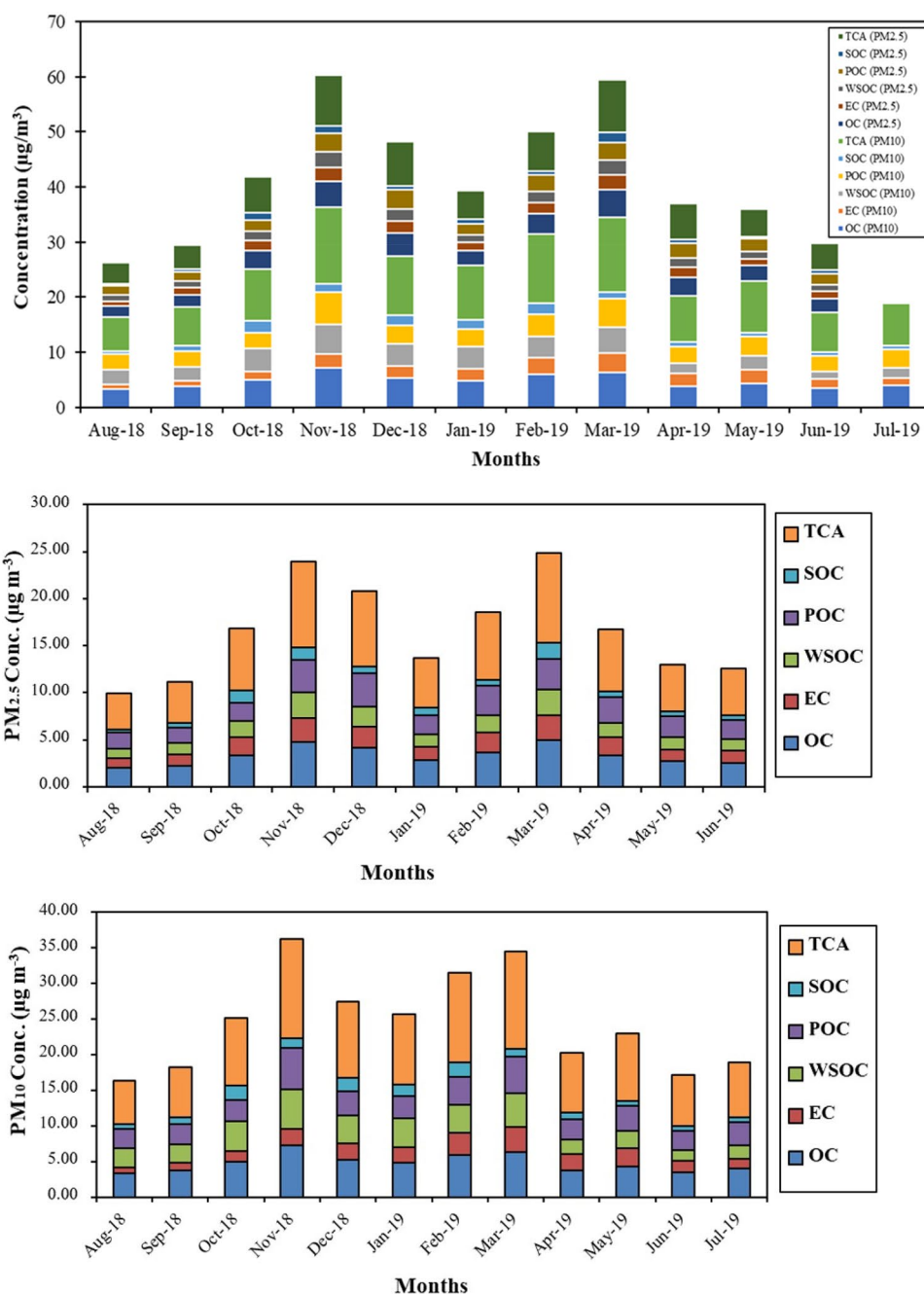
The OC/EC ratio varies significantly from source to source due to the varying strengths of the various emission sources (Yang et al. 2019). Besides, the presence of a minimum OC/EC ratio indicates that samples contain almost entirely primary carbonaceous compounds which can be influenced by various factors such as meteorology, local sources, and long-range aerosol transport (Dinoi et al. 2017). In India, biomass burning emissions (from wood fuel, agriculture waste, and cow dung) have been reported as a major contributor of carbonaceous aerosols, while coal-based emissions are predominant in eastern India (Ram and Sarin 2010). The OC/EC ratios ranged from 1.05 to 2.87 in PM_{2.5} and 1.27 to 5.25 in PM₁₀. The average OC/EC ratio in PM_{2.5} (Table 2) was higher in post-monsoon (1.94 ± 0.45) > pre-monsoon (1.92 ± 0.36) > winter (1.87 ± 0.36) > monsoon (1.85 ± 0.41); whereas for PM₁₀, monsoon (3.37 ± 1) > post-monsoon (3.01 ± 0.9) > winter (2.04 ± 0.37) > pre-monsoon (1.74 ± 0.30). The higher OC/EC highlights the clear prevalence of the organic carbon species over EC, whereas the low ratio indicates the higher emissions from fossil fuel (coal and vehicular exhaust) combustion in Darjeeling. This may be attributed to local heating systems and biomass burning which is an important source of primary-originated OC (Sharma et al. 2021).

The complexity of the OC reaction pathways, as well as the large number of products produced by photochemical and thermal oxidation reactions, may render in the quantification of SOC contributions to carbonaceous aerosol (Dinoi et al. 2017). Atmospheric VOCs, which undergo gas-to-particle conversion in the presence of some oxidizing agents (ozone, hydroxy radicals, free radicals of oxides of nitrogen) and solar radiation, are essential for the formation of SOA in the atmosphere (Alves and Pio 2005). The higher ratio of SOC/OC (Table 2) indicates the high contribution of SOC to OC, and vice versa. In the present study, the higher ratio of SOC/OC was observed in post-monsoon for PM_{2.5} (0.44 ± 0.12) and monsoon for PM₁₀ (0.48 ± 0.16) can be attributed to increased emissions of volatile organic precursors, combined with a stable atmosphere and longer

residence time, which may strengthen atmospheric oxidation of volatile organic compounds. During study, the lowest ratio of SOC/OC was observed in winter (0.23 ± 0.13) for PM_{2.5} and pre-monsoon (0.25 ± 0.11) for PM₁₀ may be attributed to direct emissions from combustion sources (coal and other fossil fuel combustion).

WSOC is one of the key components of carbonaceous aerosols because it contributes to the density of the cloud condensation nucleus (CCN) which can influence the global climate (Jin et al. 2020). The WSOC/OC (Table 2) ratios ranged from 0.22 to 0.78 and 0.18 to 0.81 with an average of 0.52 ± 0.16 and 0.69 ± 0.21 for PM_{2.5} and PM₁₀, respectively. In PM₁₀, the average of WSOC/OC was quite high that may come from cement dust, soil dust, and biogenic aerosols such as algae, pollen, etc. A broad range of WSOC/OC ratios indicates that emission sources, their intensity, and the contribution of SOA at the sampling site are all vulnerable to temporal variability (Ram et al. 2012). When compared to emissions from biomass burning, the vehicle emissions ratios of WSOC/OC are typically low because of poor solubility for organic fuels such as diesel, gasoline, etc. Besides, Ho et al. (2007) suggested that WSOC/OC ratios are used as an indicator for the formation of secondary aerosols and the presence of aged aerosols, which can further transport over long distances. The average WSOC/OC was found to be 0.50 and 0.71 in winter, 0.52 and 0.61 in pre-monsoon, 0.53 and 0.65 in monsoon, and 0.54 and 0.79 in post-monsoon for PM_{2.5} and PM₁₀, respectively. The highest WSOC/OC was observed in the post-monsoon season indicating the enhanced contribution of fresh secondary aerosols, as shown in our previous study (Rai et al. 2020). This may be due to the aging of organic compounds and being absorbed by the atmosphere during the production of secondary organic aerosols (SOA). A correlation between WSOC and OC was observed to evaluate the presence of secondary aerosols, as shown in Fig. S4 (in supplementary information). A very significant correlation was found in pre-monsoon ($R^2=0.91$, $R^2=0.73$ with $p<0.05$), and post-monsoon ($R^2=0.85$, $R^2=0.83$ with $p<0.05$) in PM₁₀ and PM_{2.5}, respectively, suggesting the abundance of emissions of secondary

Fig. 4 Monthly average concentrations of carbonaceous species (OC, EC, WSOC, POC, SOC, TCAs) of $PM_{2.5}$ and PM_{10} over Darjeeling



aerosols. Whereas, weaker correlation in winter ($R^2=0.58$, $R^2=0.63$ with $p<0.05$) and monsoon ($R^2=0.17$, $R^2=0.62$ with $p<0.05$) in PM_{10} and $PM_{2.5}$ was observed indicating the presence of different emission sources.

3.2 Transport Pathway of $PM_{2.5}$ and PM_{10}

3.2.1 Backward Trajectory Analysis

The techniques of trajectory modeling provide an analytical and visually compelling way to classify geographical regions

associated with the long-range transport of pollutants to particular locations. The annual (Fig. S5 in Supplementary Information) and seasonal (Fig. 6) air mass backward trajectories were plotted at the height of 100 m, 500 m, and 1000 m to understand the pathway of pollutants arriving at the sampling site of Darjeeling.

At the height of 100 m, the trajectories were expected to persist in the boundary layer throughout the year, as shown in Fig. 6 representing well-mixed air masses that lead to visibility conditions encountered at ground level. However, orographic effects and other surface features are more strongly

Fig. 5 Seasonal average concentration of carbonaceous species (OC, EC, WSOC, POC, SOC, TCAs) of PM_{2.5} and PM₁₀ over Darjeeling

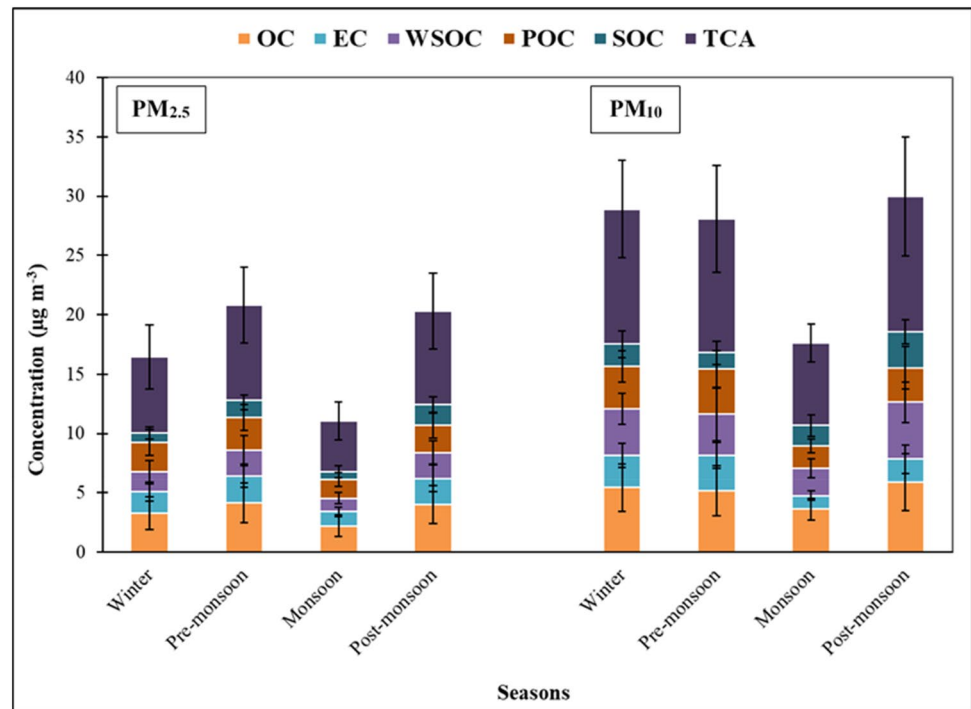


Table 2 Average ratio of PM_{2.5} and PM₁₀, and OC/EC, WSOC/OC, and SOC/OC of PM_{2.5} and PM₁₀ in Darjeeling

Season	PM _{2.5} /PM ₁₀	PM _{2.5}			PM ₁₀		
		OC/EC	WSOC/OC	SOC/OC	OC/EC	WSOC/OC	SOC/OC
Winter	0.46	1.87 ± 0.36 (1.4)	0.50 ± 0.18	0.23 ± 0.13	2.04 ± 0.37 (1.31)	0.71 ± 0.19	0.33 ± 0.13
Pre-monsoon	0.42	1.92 ± 0.36 (1.22)	0.52 ± 0.17	0.35 ± 0.11	1.74 ± 0.30 (1.27)	0.61 ± 0.19	0.25 ± 0.11
Monsoon	0.13	1.85 ± 0.41 (1.3)	0.53 ± 0.17	0.27 ± 0.14	3.37 ± 1.00 (1.62)	0.65 ± 0.20	0.48 ± 0.16
Post-monsoon	0.69	1.94 ± 0.45 (1.05)	0.54 ± 0.11	0.44 ± 0.12	3.01 ± 0.90 (1.5)	0.79 ± 0.10	0.47 ± 0.10

Values in parentheses are minimum

± Standard deviation

influenced by these trajectories and appear to cluster along defined paths, and many trajectories drift as they are triggered by localized surface flows (NESCAUM 2002). Consequently, the air parcel transporting from the IGP, central highlands of India, Nepal, Bay of Bengal (BoB) contributes to regional pollution. By dividing these trajectories into different seasons, the local pollution sources are observed in pre-monsoon and winter seasons; monsoon brings the air masses from the semi-arid region and BoB; post-monsoon and winter show transport of some transboundary pollutants.

The 500 m trajectories are distributed more evenly throughout the south and west with a smaller number of trajectories indicating the shallow surface flows exhibiting a characteristic of chaotic behavior (NESCAUM 2002). Heavy air mass loading at the height of 500 m was observed at the IGP region located below the sampling location that originates from the Thar desert, semi-arid region, central highlands, Nepal, Sikkim as western pollutants, Assam and

BoB from eastern and southern contaminants, respectively (Fig. 6). The seasonal transport of pollutants demonstrates the arrival of a significant proportion of aerosols from the IGP region. During pre-monsoon, the Thar desert, semi-arid region, north-east region of Nepal, and Sikkim contribute to pollutant transport; whereas, for the post-monsoon season, Sikkim and the IGP region were the main pollutant emitters. Moreover, monsoon brings pollutants from the semi-arid region, central highlands, north-east region (Assam), and the BoB, whereas winter brings from semi-arid, central highlands, and Sikkim.

The general pattern of high-altitude trajectories (above the boundary layer) is consistent with a strong impact of upper-level winds in the free troposphere. However, the pathway of a parcel that migrates from the boundary layer into the free troposphere may accurately reflect its route that subsides and ultimately resides in the mixed layer to represent better the source region whose emissions contribute

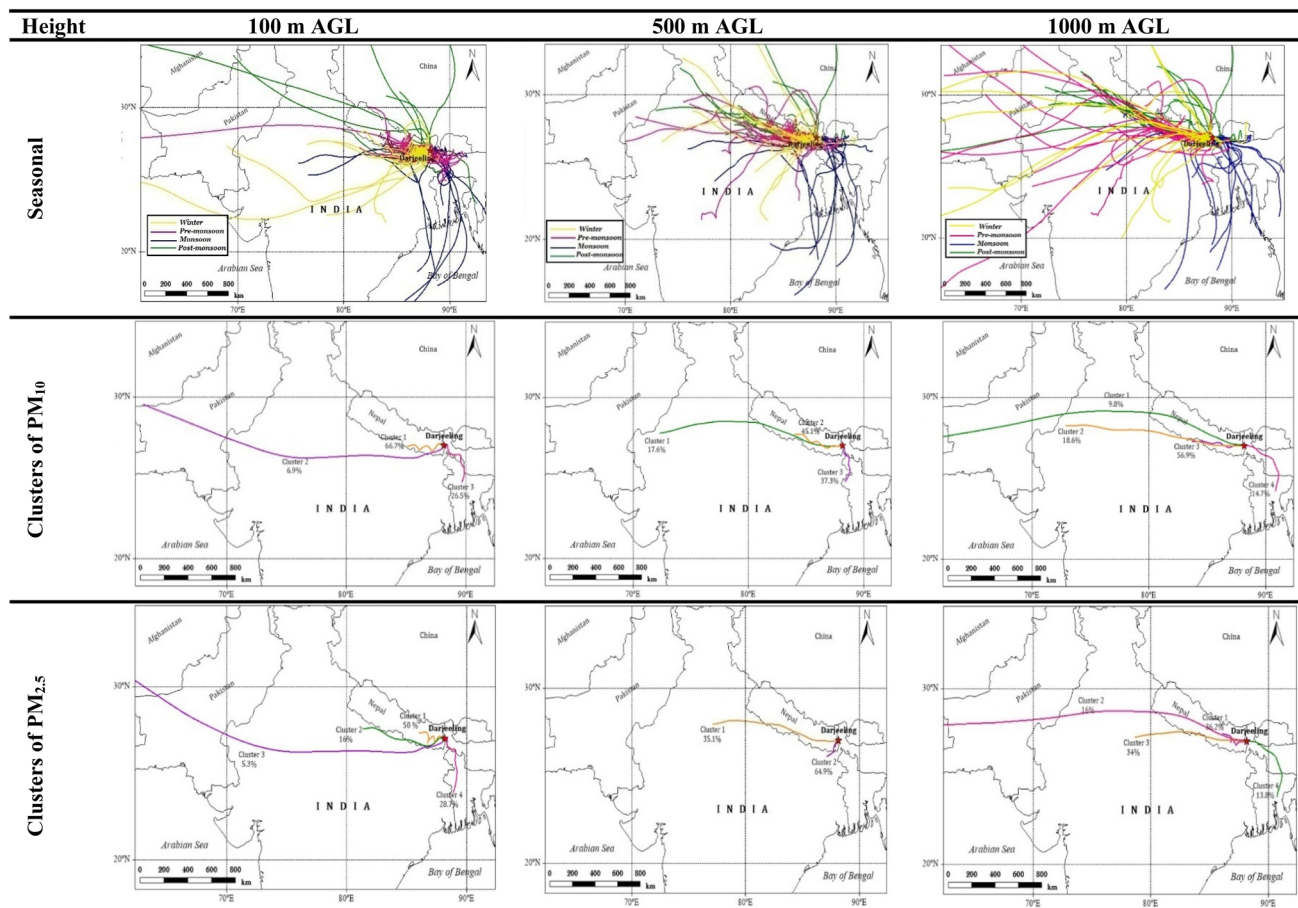


Fig. 6 Seasonal air mass backward trajectories and cluster map of PM_{10} and $PM_{2.5}$ at a height of 100 m, 500 m, and 1000 m AGL at Darjeeling

to the ambient concentrations observed at the end of the trajectory (NESCAUM 2002). At 1000 m (Fig. 6), the observed transport of air parcels was from transboundary (Afghanistan, Pakistan, Iran, and other south-western countries), marine (the Arabian Sea and BoB), as well as regional (the Thar desert, central highlands, IGP region, north-east region) sources. Winter contributes aerosols from south-western countries as transboundary, Deccan plateau, and local source of pollutants as regional. Monsoon carries aerosols from the IGP, BoB, and north-east regions (Assam and Myanmar). Pre-monsoon loads pollutants from central Asian countries (Afghanistan, Pakistan, Iran), the IGP region, and central highlands, whereas post-monsoon transport pollutants from Pakistan, IGP, and China.

3.2.2 Cluster Analysis

Cluster analysis was conducted at various altitudes (100 m, 500 m, and 1000 m) to compare the prevailing patterns of air mass backward trajectories and each pattern's frequency. The altitude variation influences the percentage of paths in each cluster, reflecting their mean trajectory (Su et al. 2015;

Ghosh et al. 2015). The percentage is much higher in local pathways than in comparatively long-distance clusters compared with a higher altitude (Su et al. 2015; Ghosh et al. 2015). The clusters of annual trajectories were mapped at all heights (100 m, 500 m, 1000 m) for both $PM_{2.5}$ and PM_{10} , as demonstrated in Fig. 6. The total number of trajectories assigned to each group with their number of polluted trajectories, frequency, and mean PM concentrations are summarized in Table 3. The number of polluted trajectories implies the trajectories cohering with PM equivalent to or greater than NAAQS (India) with a limiting value of $60 \mu\text{g m}^{-3}$ and $40 \mu\text{g m}^{-3}$ for PM_{10} and $PM_{2.5}$. The long-range transport pathways of PM_{10} depend primarily on the atmospheric advection movement (Chen et al. 2018). Fine PM, on the other hand, has prolonged atmospheric residence time that leads to the contribution in secondary aerosols formation which is produced within the atmosphere by various chemical/physical processes (WHO Joint, 2006).

The cluster map plotted at the height of 100 m gives 3 clusters for PM_{10} and 4 clusters for $PM_{2.5}$ (Fig. 6). Cluster 3 is the lowest frequency trajectory (5.3%) in $PM_{2.5}$ and reflects long-range transport from the Middle East countries.

Table 3 Cluster statistics of each cluster and corresponding mean concentrations of PM_{2.5} and PM₁₀ (μg m⁻³) at different heights (100, 500, 1000 m AGL)

	Height (AGL)	Cluster	Trajectory Number	Frequency (%)	PM Concentration (μg m ⁻³)	Polluted trajectories	Polluted trajectory frequency (%)	Polluted Mean PM concentration (μg m ⁻³)	
PM _{2.5}	100 m	1	46	50	36 ± 16	14	30	11 ± 5	
		2	15	16	42 ± 11	7	47	20 ± 5	
		3	5	5.3	36 ± 18	1	20	7 ± 4	
		4	27	28.7	37 ± 11	10	37	14 ± 4	
	500 m	1	33	35.1	41 ± 12	17	52	21 ± 6	
		2	60	64.9	35 ± 12	15	25	9 ± 3	
	1000 m	1	33	36.2	37 ± 11	10	30	11 ± 3	
		2	15	16	39 ± 16	6	40	16 ± 6	
		3	32	34	38 ± 12	10	31	12 ± 4	
		4	13	13.8	38 ± 11	6	46	18 ± 5	
	PM ₁₀	100 m	1	68	66.7	57 ± 20	25	37	21 ± 7
			2	7	6.9	50 ± 12	2	29	14 ± 3
3			27	26.5	53 ± 12	7	26	14 ± 3	
4			13	13.8	38 ± 11	6	46	18 ± 5	
500 m		1	18	17.6	61 ± 15	10	56	34 ± 8	
		2	46	45.1	59 ± 22	20	43	26 ± 10	
		3	38	37.3	49 ± 10	4	11	5 ± 1	
1000 m		1	10	9.8	67 ± 26	6	60	40 ± 16	
		2	19	18.6	66 ± 16	12	63	42 ± 10	
		3	58	56.9	51 ± 17	14	24	12 ± 4	
		4	15	14.7	50 ± 9	2	13	7 ± 1	

± Standard deviation (at ± 1σ)

The highest frequency of trajectories (50%) leading to about 30% of polluted trajectories demonstrated by Cluster 1. The highest mean PM_{2.5} concentration (42 ± 11 μg m⁻³) in cluster 2 was derived from the most polluted IGP region. The cluster maps of PM₁₀ also depict the highest frequency trajectory (66.7%) and mean PM₁₀ concentration (57 ± 20 μg m⁻³) originating from Nepal with ~37% of polluted trajectories, as illustrated in cluster 1. Cluster 2 is the lowest frequency trajectory (6.9%), demonstrating long-range transport from Central Asian countries (Afghanistan and Pakistan).

Trajectories are mapped at 500 m in height into 2 clusters of PM_{2.5} and 3 clusters of PM₁₀ (Fig. 6). In PM_{2.5} maps, cluster 2 of 64.9% comes primarily from the middle IGP region, while cluster 1 is derived from the lower IGP region carrying approximately 52% of polluted trajectories at a mean of 41 ± 12 μg m⁻³. For PM₁₀, cluster 2 is the main contributor to polluted trajectories (~43%) of 45% originated from Nepal. Besides, cluster 1 contributes maximum mean concentration of PM₁₀ (61 ± 15 μg m⁻³) indicating medium-range transport of pollutant from the Thar desert. The dust was carried to downstream regions and airflow, contributing to dust storm conditions (Chen et al. 2018).

For the upper boundary layer and the low free troposphere that offers the most prominent clusters, a similar analysis was performed. Four clusters were found at higher altitudes of

1000 m with PM_{2.5} and PM₁₀ (Fig. 6). Cluster 1 of PM_{2.5} and PM₁₀ denotes the highest frequency of trajectories at 1000 m with 36.2% and 56.9% of pollutants loading, respectively, transported from the Nepal; whereas, cluster 2 represents 30% and 24% of air mass loading in PM_{2.5} and PM₁₀ that arises from the Nepal-IGP area, respectively. The lowest trajectory frequency contribution of PM_{2.5} (13.8%) and PM₁₀ (9.8%) was recorded from Bangladesh (through south-western monsoon pattern) and far western countries (through western winds), by cluster 4 and cluster 1, respectively. The mean PM_{2.5} concentration was almost the same for cluster 2 (39 ± 16 μg m⁻³); while for PM₁₀, clusters 3 and 4 assessed nearly the same mean concentration with the highest in cluster 1 (67 ± 26 μg m⁻³).

The results of the cluster analysis concluded that the HYSPLIT trajectory is susceptible to data resolution, when the pollutants transport from short-range (west or south-east), and when the air transports from medium (western) and long-range (north-western), the trajectories are more able to persist unaffected with variations in vertical speed.

3.2.3 Seasonal CWT of PM_{2.5}, PM₁₀ and Carbonaceous Species

It is evident from the above results that the sampling site is affected by mixed types of pollutants (influenced by

continental, local, and marine inflow). Sarkar et al. (2015) show that the influence of local pollution on Darjeeling was substantially more potent than other high-altitude Himalayan stations, which may be attributed to high anthropogenic emissions from tourism, high population density, unplanned settlements, and also a unique orography and landform with narrow roads led to lack of ventilation and dispersion of aerosols. Adak et al. (2013) reported that the fine mode aerosols were mostly anthropogenic aerosols produced locally. For each of the determined chemical species, the CWT model was applied separately by assigning the measured concentrations to grids concentrated in 'hot spots' that were used as tracers of particular types of PM emissions (Dimitriou et al. 2015, 2020). The grid with a higher value signifies the dangerous effect of particulate and carbonaceous aerosols on the location. To better identify significant pollution regions, only grids with high CWT values were designated (Li et al. 2020b). The well-mixed convective boundary layer (500 m) was studied to reduce the impact of surface turbulence (Yang et al. 2017). Figure 7 depicted a CWT map for Darjeeling with PM₁₀ and PM_{2.5} concentrations in winter, pre-monsoon, monsoon, and post-monsoon from August 2018 to July 2019. Also, Figs. 8, 9, 10, 11, 12, 13 depicted a CWT map for Darjeeling of OC, EC, TCA, POC, SOC and WSOC concentrations of PM₁₀ and PM_{2.5} in winter, pre-monsoon, monsoon, and post-monsoon. The CWT maps of PM₁₀ and PM_{2.5} (Figs. S6–S8) along with their OC (Figs. S9–S11), EC (Figs. S12–S14), POC (Figs. S15–S17), SOC (Figs. S18–S20), WSOC (Figs. S21–S23) and TCA (Figs. S24–S26) at a height of 100 m, and 1000 m are shown in the supplementary information.

3.2.3.1 Winter Among all seasons, the winter season recorded the lower concentrations for both PM₁₀ and PM_{2.5} emitted from incomplete combustion of fuels and wood at low temperature, used to combat chills. A persistent thermal inversion with limited dispersion is formed at ground level due to calm wind and fog conditions that entrapped a greater number of fine pollutants i.e., PM_{2.5} (59%). From the observed results, a higher EC average concentration of $2.7 \pm 1.0 \mu\text{g m}^{-3}$ in PM₁₀ and $1.8 \pm 0.8 \mu\text{g m}^{-3}$ in PM_{2.5} may attributable to combustion activities such as biomass, fuels, and wood (for heating purposes) and coal (from "Toy Train") over Darjeeling. Li et al. (2020a) have reported the complexity of OC sources which include combustion, fine soil particles, pollen, and secondary organic processes. The average OC concentration of PM₁₀ and PM_{2.5} in the present study were 12.34 and $5.87 \mu\text{g m}^{-3}$, varying from 2.09 to $12.34 \mu\text{g m}^{-3}$ and 1.04 to $5.87 \mu\text{g m}^{-3}$, respectively. The POC contributes maximum to OC of PM₁₀ (65%) and PM_{2.5} (76%) emitted predominantly from eastern Nepal and local Darjeeling areas, along with a smaller amount of PM_{2.5} SOC. In contrast, the IGP, Nepal, and the central highlands

were transporting over $2 \mu\text{g m}^{-3}$ of SOC of PM₁₀. Due to the incidence of forest fires in Pakistan, the IGP region, the north-eastern and southern parts of India, MODIS fire spots showed good agreement with the observed results (Fig. 14). In the sampling region, the air was polluted by a forest fire and biomass burning fumes as well as continental air mass. Tripathee et al. (2021) indicated that wintertime aerosols in Dhulikhel (Nepal) mainly consist of polluted continental air mass that comprises dust and smoke. Furthermore, WSOC also contributes a fraction of the OC that shows a similar EC trend, that might be emitted from biomass burning, industries, dust, and automobile emissions and form secondary organic aerosol (SOA) (Sharma et al. 2021; Jin et al. 2020). Therefore, the contribution of TCAs is approximately 21% of PM₁₀ and PM_{2.5} each is primarily from the IGP region, Nepal, and local region. Following the harvest of wheat crops every April–May in the IGP region, large-scale wheat-residual burning is the main source of biomass burning emissions which can emit numerous organic particles (Yuan et al. 2020b).

3.2.3.2 Pre-monsoon In Darjeeling, the peak tourist season is the pre-monsoon which contributes to the highest concentrations of PM and its carbonaceous species. The majorly polluted regions (western Nepal and IGP) with the highest mean concentration of PM₁₀ and PM_{2.5} exceeded the NAAQS standard limit as shown in Fig. 7. This could be due to the long-range transport of dust aerosol, nucleating vapors, and precursor gases driven by westerly winds from arid and semi-arid regions of western India and Asia, including the Thar Desert and Arabian deserts, respectively (Rai et al. 2020; Chatterjee et al. 2010; Adak et al. 2013). Moreover, the formation of fine particles in Darjeeling is favored by weather conditions including increased solar radiation and relative humidity (Adak et al. 2013). EC is one of the PM components indicating the presence of pollution from tourist vehicles, dust, smoke, and combustion of coal in the "Toy Train" of DHR. In the current review, the EC concentration of PM₁₀ covers a larger area of Nepal with more than $1.6 \mu\text{g m}^{-3}$ compared to PM_{2.5}. Our observations are consistent with the recent research on Dhulikhel (Nepal) by Tripathee et al. (2021). With more than $4 \mu\text{g m}^{-3}$ over Nepal, pre-monsoon is the largest contributor of OC of PM₁₀ in comparison to PM_{2.5}. A similar emission trend of POC, SOC, and WSOC of PM₁₀ was observed from Nepal, IGP, and local regions contributing 73%, 26%, and 66% to OC, respectively. In another case of PM_{2.5}, the least SOC concentration and high emissions of POC (65%) and WSOC (53%) were measured among all seasons. This implies that various anthropogenic activities such as combustion of various types of fuels, biomass burning, and forest fire, vehicular emission and pollutants from Darjeeling Himalayan railway (due to influx of tourist) may result in emissions of higher

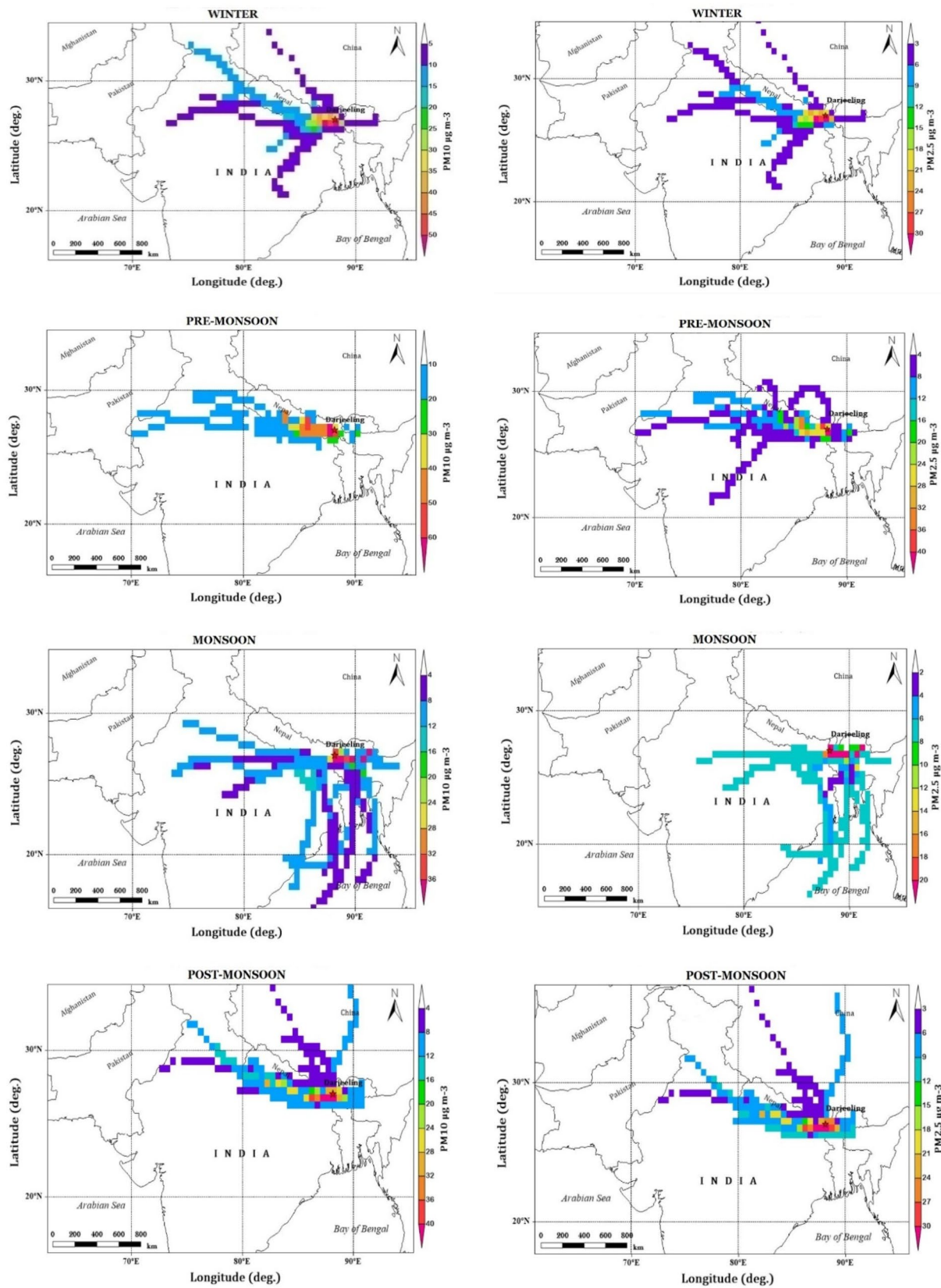


Fig. 7 Seasonal CWT analysis of PM₁₀ (left panel) and PM_{2.5} (right panel) (in $\mu\text{g m}^{-3}$) at 500 m AGL

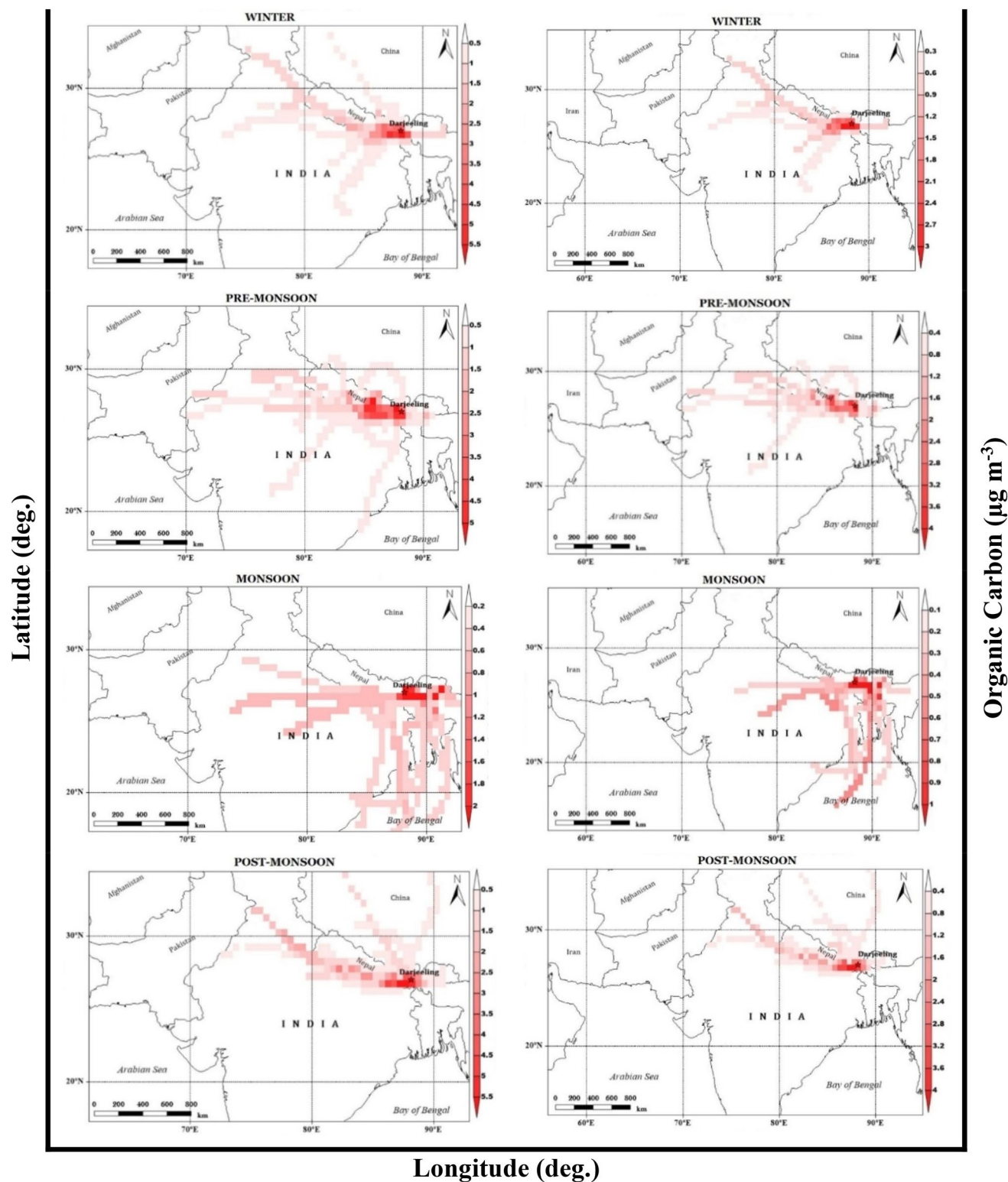


Fig. 8 Seasonal CWT analysis of OC of PM_{10} (left panel) and $PM_{2.5}$ (right panel) (in $\mu\text{g m}^{-3}$) at 500 m AGL

number of organic aerosols. Dust aerosols from the IGP region are vertically advected due to increased convection and pressure gradient, and arrive at the foothills of the Him-

alayas, combined with carbonaceous species (Adak et al. 2013; Chatterjee et al. 2010). Furthermore, active Terra and Aqua MODIS fire and thermal anomalies ($\geq 80\%$) indicate

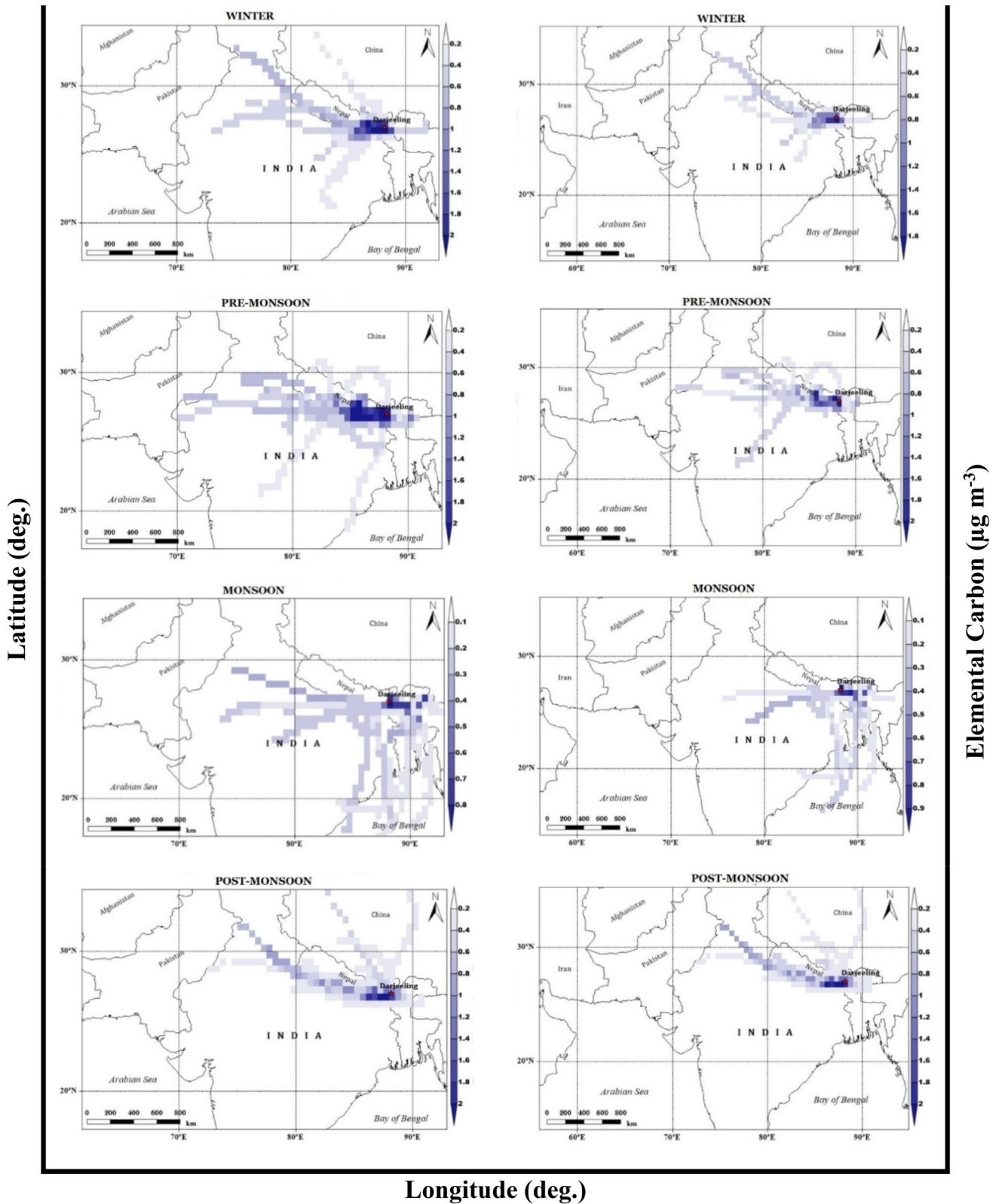


Fig. 9 Seasonal CWT analysis of EC of PM_{10} (left panel) and $\text{PM}_{2.5}$ (right panel) (in $\mu\text{g m}^{-3}$) at 500 m AGL

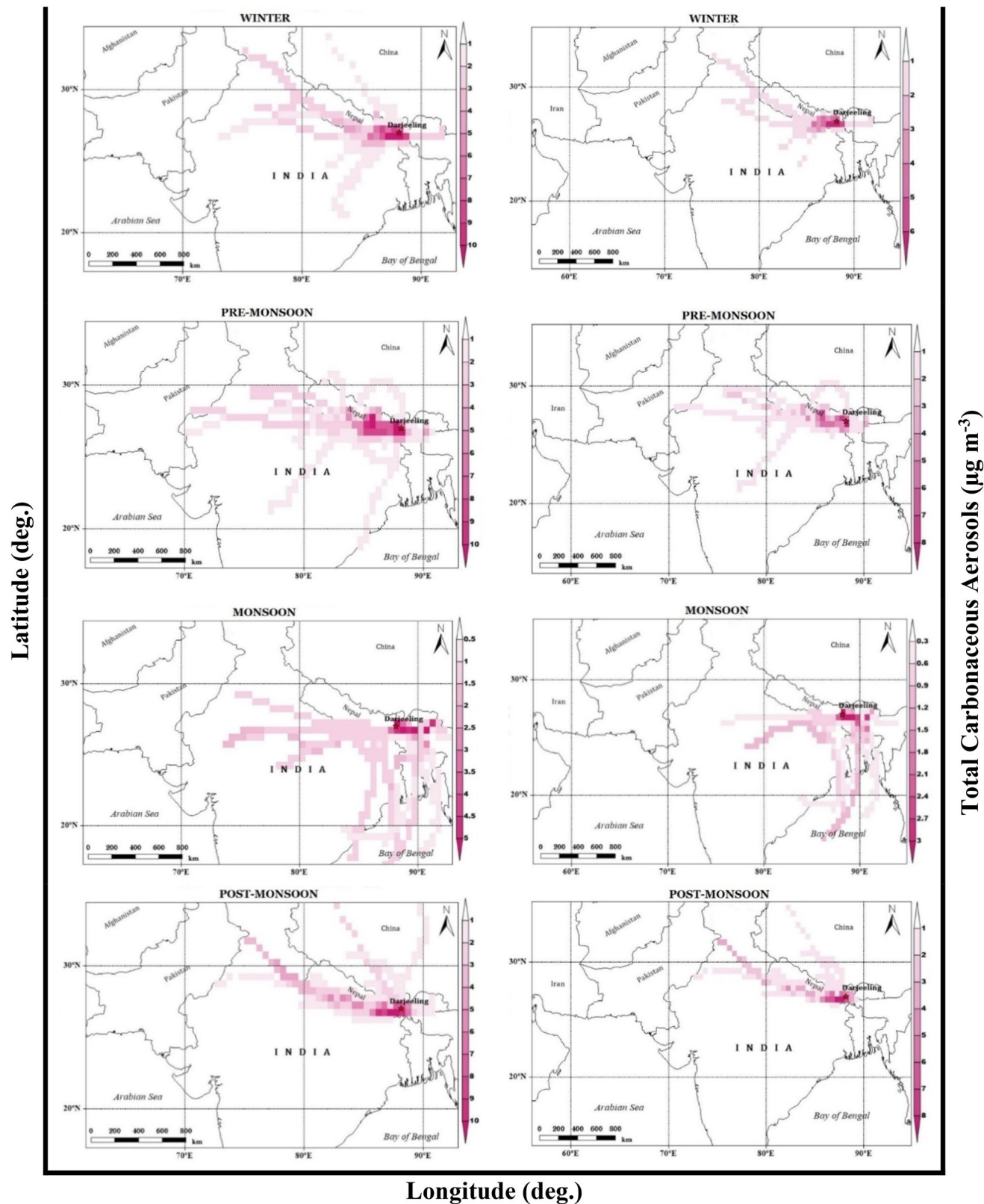


Fig. 10 Seasonal CWT analysis of TCAs of PM₁₀ (left panel) and PM_{2.5} (right panel) (in $\mu\text{g m}^{-3}$) at 500 m AGL

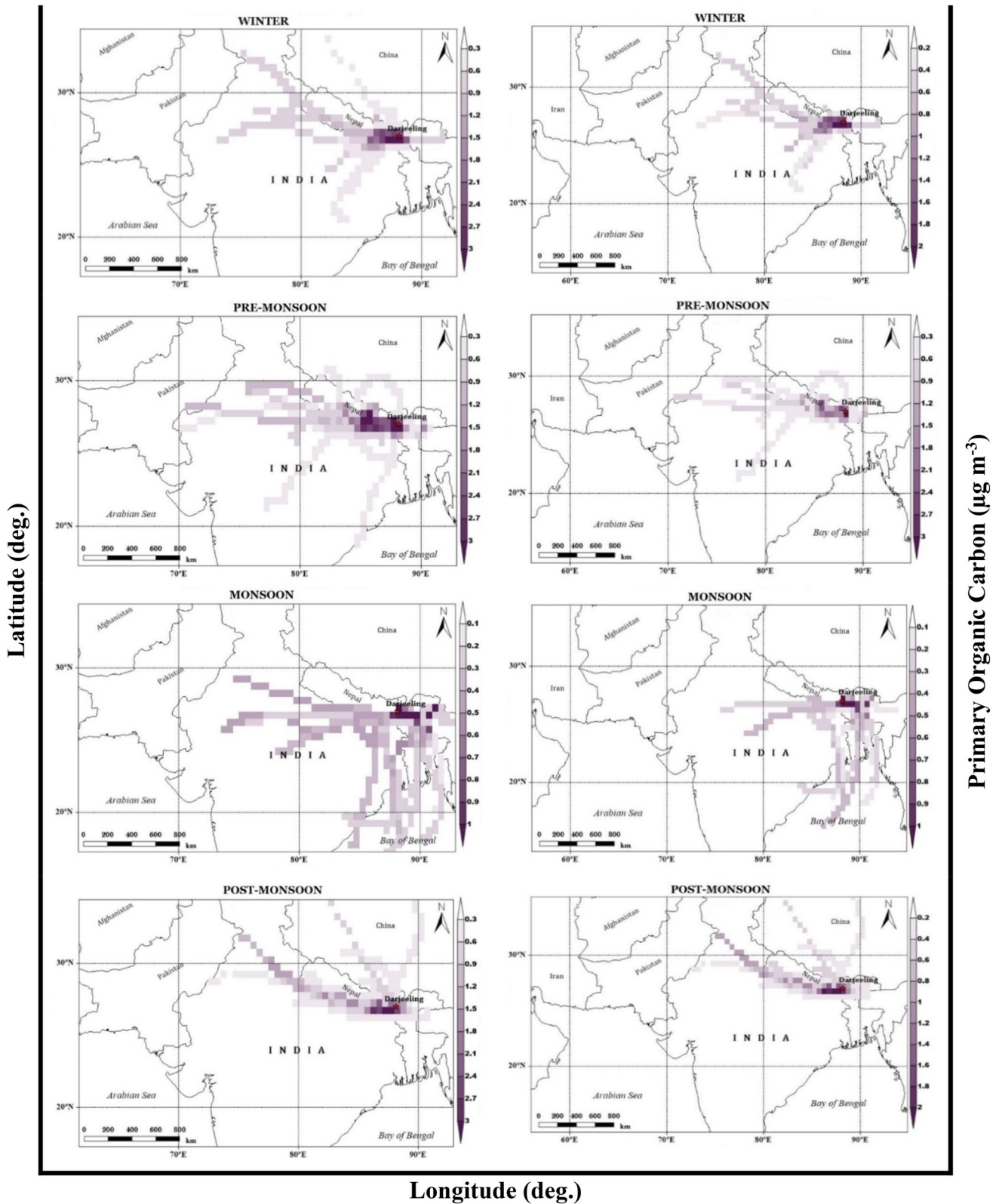


Fig. 11 Seasonal CWT analysis of POC of PM_{10} (left panel) and $\text{PM}_{2.5}$ (right panel) (in $\mu\text{g m}^{-3}$) at 500 m AGL

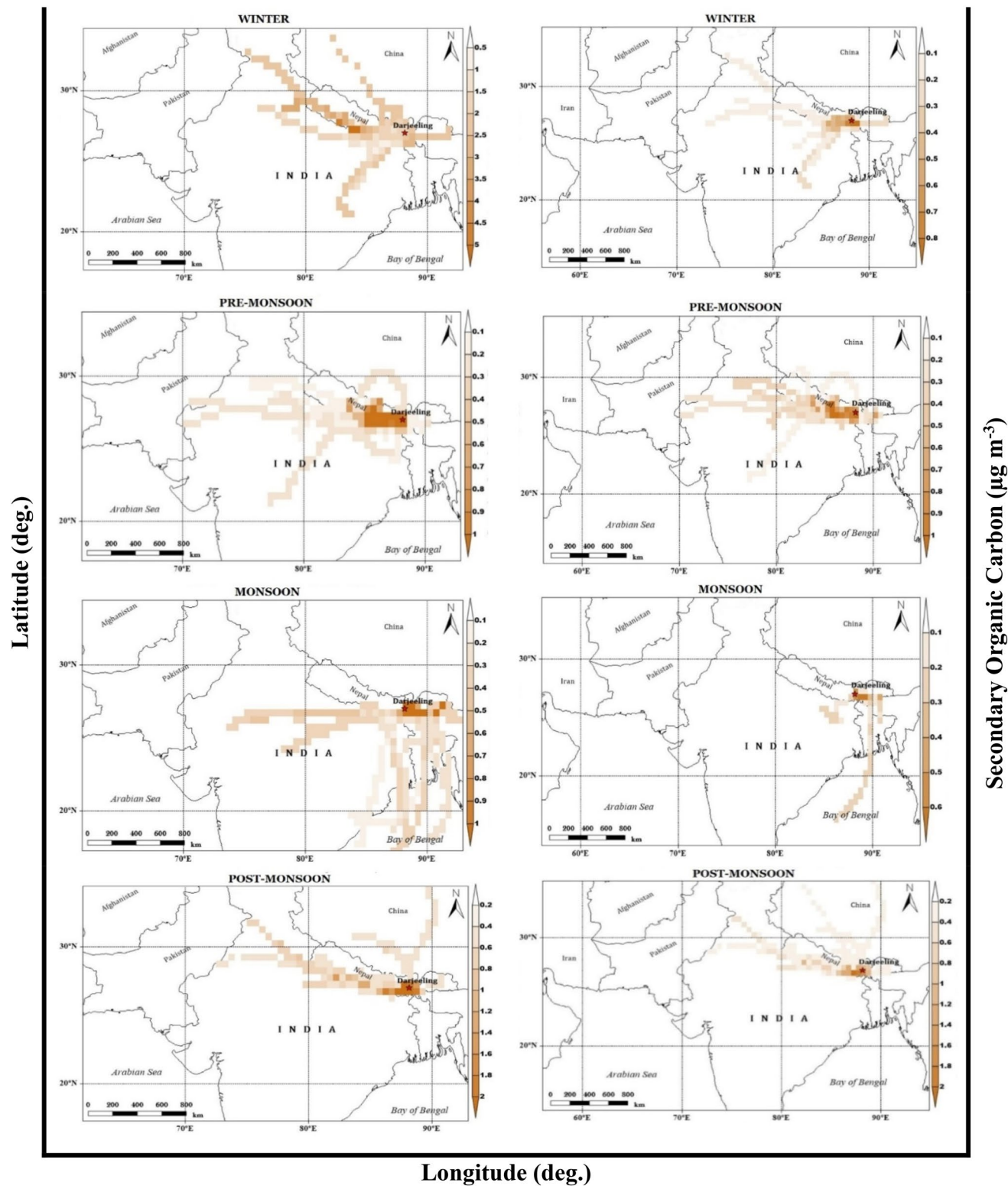


Fig. 12 Seasonal CWT analysis of SOC of PM_{10} (left panel) and $PM_{2.5}$ (right panel) (in $\mu\text{g m}^{-3}$) at 500 m AGL

the prevalence of forest fires across India except in the Thar Desert of Rajasthan and fewer in Bihar and Bangladesh (Fig. 14). Consequently, due to the influx of visitors, the

increased anthropogenic activities in Darjeeling and neighboring areas, the contribution of TCA in PM_{10} and $PM_{2.5}$ is almost 18% and 20%. Although the contribution appears to

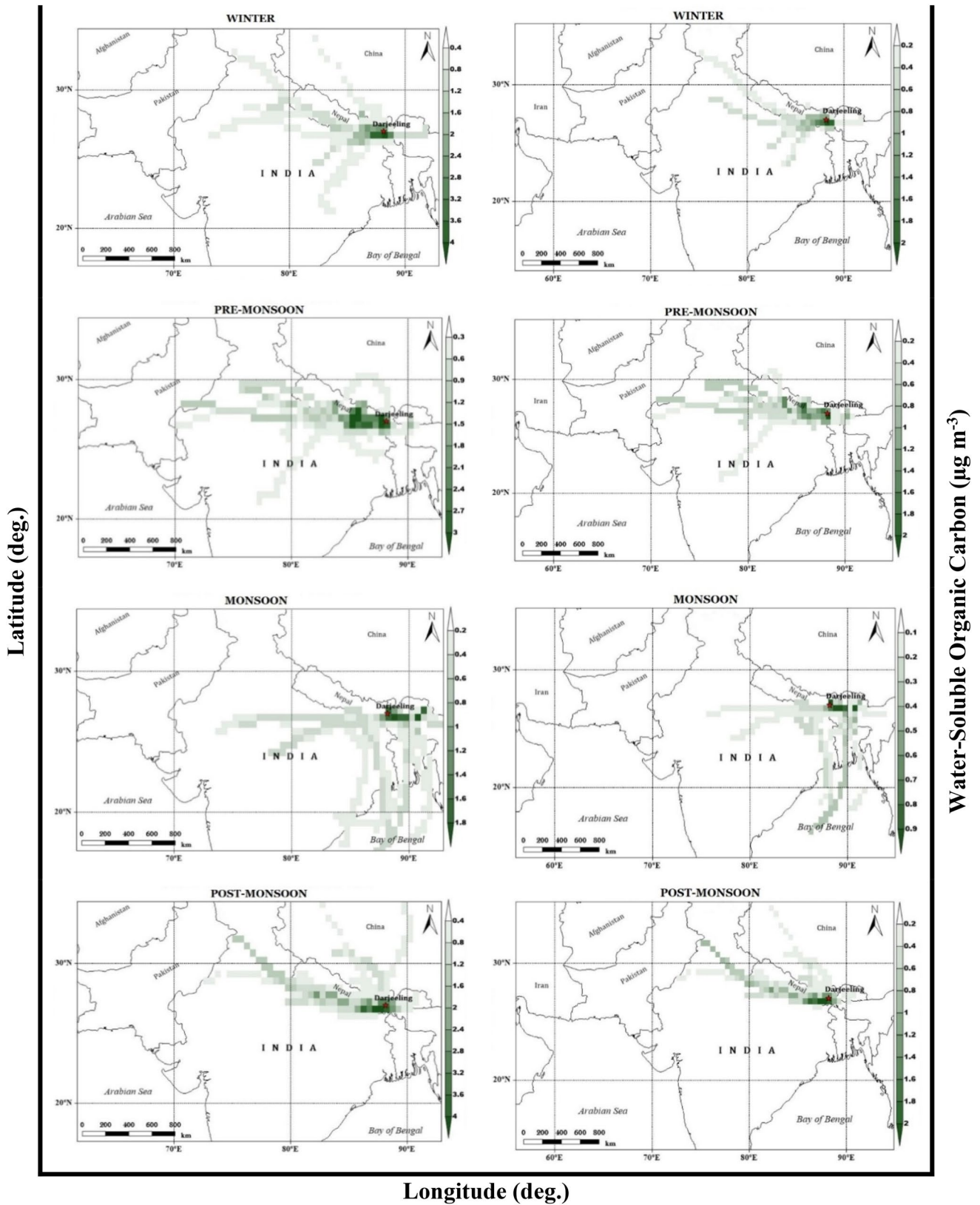


Fig. 13 Seasonal CWT analysis of WSOC of PM_{10} (left panel) and $PM_{2.5}$ (right panel) (in $\mu\text{g m}^{-3}$) at 500 m AGL

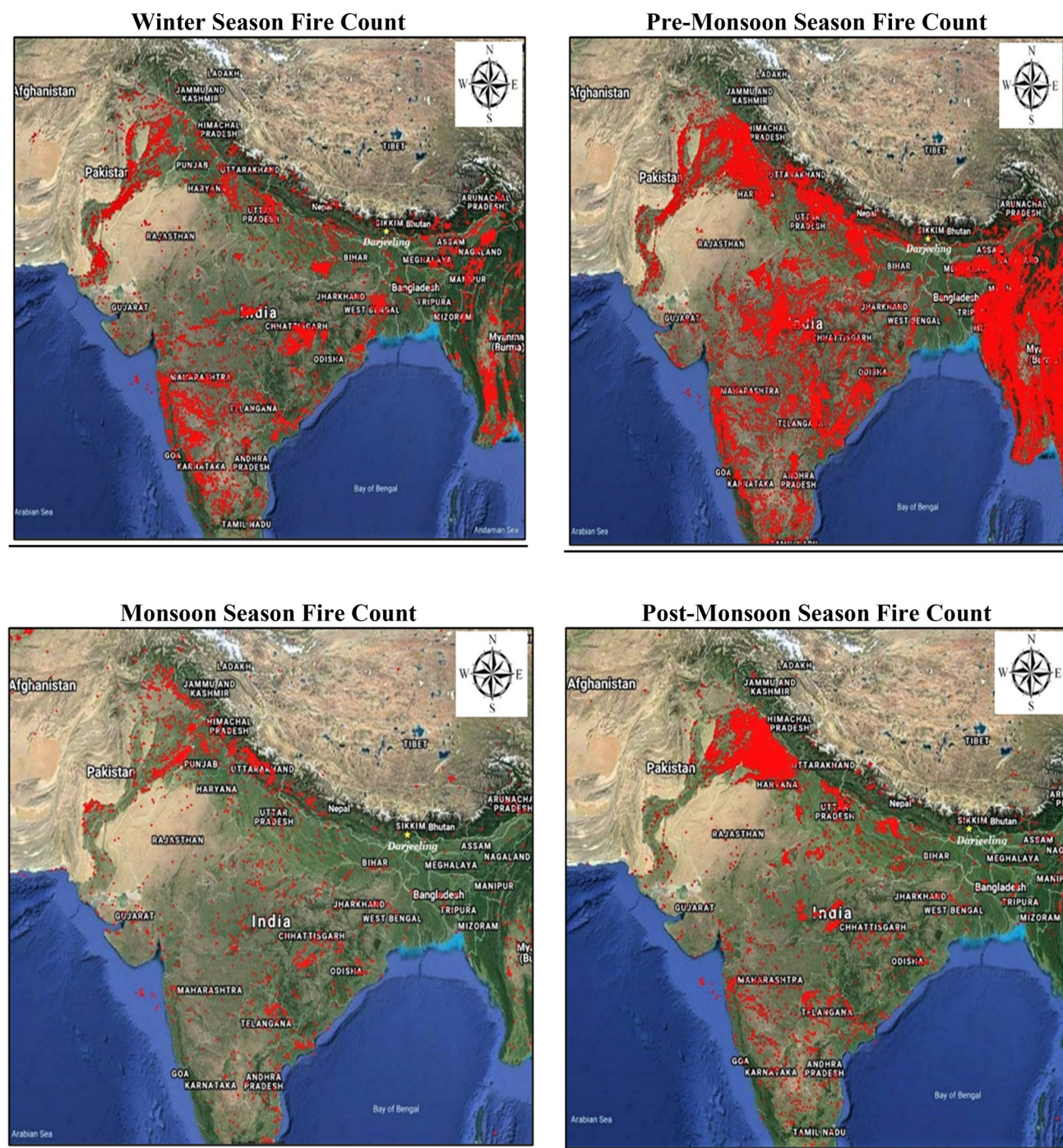


Fig. 14 Seasonal fire count map of India during August 2018–July 2019

be smaller in number, these aerosols may undergo a variety of atmospheric processes leading to the formation of toxic pollutants in the presence of favorable conditions.

3.2.3.3 Monsoon High precipitation in the foothills of the eastern Himalayas is due to their proximity to the BoB and their direct exposure to the moisture-laden mountain pat-

terns of the southwest monsoon zone (Cajee 2018). The monsoon season depicts the effect of air masses vertically elevated from the BoB and horizontally transported by convective motion through the southerly flow to the Himalayas (Chatterjee et al. 2010). Although, the possible origin of marine and continental aerosols leads to the influence of mixed aerosols over Darjeeling with minimum concen-

trations of PM and its carbonaceous components. During the monsoon, almost equal concentrations of EC of PM_{2.5} and PM₁₀ were measured that might be attributed to fossil fuel combustion and vehicular exhaust. The average OC concentration of PM_{2.5} and PM₁₀ was $3.6 \pm 1.6 \mu\text{g m}^{-3}$ and $5.1 \pm 2.0 \mu\text{g m}^{-3}$ contributing to significant biomass burning from the IGP region, central highlands, BoB, Bangladesh, Assam, and Bhutan. In the north-western Himalayas, Eastern Ghats, and a few central highways and the IGP region, MODIS fire spots supported observed findings (Fig. 14). Due to the below-cloud scavenging process, low concentrations of WSOC and SOC were observed with less than $1 \mu\text{g m}^{-3}$. The contribution of POC to the OC of PM₁₀ (51%) and PM_{2.5} (71%) is strongly influenced by local emissions, the IGP region, and Nepal. The TCAs load of the PM is ~11–13% over the IGP region, BoB, and north-eastern region of India that may be attributed to dust and marine aerosols. Heavy precipitation and significant fall in finer mode aerosol particles indicate the washing out of aerosols; whereas, a comparatively higher concentration of coarser aerosols might be due to the influence of sea salt aerosols (Na⁺, Mg²⁺) as described in a previous study by Chatterjee et al. (2010). Results observed were close to previous studies (Adak et al. 2013; Sarkar et al. 2015, 2019; Roy et al. 2016) showing that the effect of wet scavenging and restricts the impact of long-distance transport and local pollution. The heavy dust loading significantly diminishes due to aerosol wash-out from the atmosphere.

3.2.3.4 Post-monsoon The huge influx of tourists visits Darjeeling in the post-monsoon and is known as the second peak tourist season. The most prominent transport regions of PM through strong westerlies were from Nepal, the Nepal–IGP border, and the local area. The highest concentration of PM is observed due to the peak tourist season, with the greatest contribution of carbonaceous aerosols that could be released due to the presence of high population density, contributing to more tourist vehicle pollution, fossil fuel burning, coal combustion (Toy Train), biomass burning, etc. Significant regions of OC and EC pollution were found to be higher in PM₁₀ ($5.9 \mu\text{g m}^{-3}$) and PM_{2.5} ($2.2 \mu\text{g m}^{-3}$), respectively, arriving from the IGP region through Nepal and local regions of Darjeeling. Tripathy et al. (2021) concluded the influence of continental air mass along with the smoke of biomass burning during the post-monsoon. MODIS active fire spots are in good agreement with these findings showing the massive burning over the IGP, primarily in Punjab and Haryana, where farmers burn crop residue (Fig. 14). The POC contributes about 49% and 57% to OC of PM₁₀ and PM_{2.5}, respectively that might be due to local biomass burning and forest fire episode of IGP. In the PM₁₀ map of SOC, SOC contribution is also very high ($> 2 \mu\text{g m}^{-3}$) compared to PM_{2.5}, which may be due to

the formation of secondary aerosols through the gas-to-particle conversion of VOC. Furthermore, a high concentration of WSOC was observed with a contribution of 80% and 54% to OC of PM₁₀ and PM_{2.5}, respectively, leading to the formation of cloud condensation nuclei (CCN) (Jin et al. 2020). Therefore, the TCA load of the PM is ~20% that might be attributed to dust and continental aerosols.

4 Conclusion

This study presents a seasonal progression of PM_{2.5} and PM₁₀ from August 2018 to July 2019, at Darjeeling, a semi-urban and sub-tropical site of the eastern Himalayan region of India. The annual concentrations of PM₁₀ ($55 \mu\text{g m}^{-3}$) and PM_{2.5} ($37 \mu\text{g m}^{-3}$) were observed to exceed the threshold value of WHO ($20 \mu\text{g m}^{-3}$ for PM₁₀; and $10 \mu\text{g m}^{-3}$ for PM_{2.5}) by ~36% and 27%, respectively, suggesting an increase in levels of coarse mode aerosols over Darjeeling.

- PM_{2.5} and PM₁₀ showed remarkable seasonal differences due to fluctuations in local weather conditions, local pollution, and long-range transport. The order of seasonal average concentration of both PM₁₀ and PM_{2.5}, was: pre-monsoon > post-monsoon > monsoon > winter. During the study period, the huge disparity in fine and coarse mode aerosol concentrations may be due to the unique orography and landform of Darjeeling and the thermodynamic conditions of the boundary layer, which either favor or hinder pollutants dispersion.
- The long-distance transport routes of particulate aerosols rely mainly on atmospheric advection movement. The seasonal air mass back trajectory at different altitudes (100, 500, 1000 m) reveal local, IGP, the Thar desert, semi-arid, central highlands, Nepal, Assam, and the BoB as the common major pollutant transporting regions affected by mixed types of pollutants (continental, local and marine).
- Clustering of backward trajectory at different altitudes (100, 500, 1000 m) for PM_{2.5} and PM₁₀ illustrates that the air masses may originate from short-, medium- and long-range transport associated with several polluted trajectories and mean concentration of PM.
- Following Terra and Aqua MODIS active fire data, the results of CWT analysis of PM (PM_{2.5} and PM₁₀) and its carbonaceous species (OC, EC, WSOC, POC, SOC, TCAs) are in good agreement. As pre-monsoon and post-monsoon are the peak season for tourists to visit, various anthropogenic activities increased in the town that leads to the emission from vehicles, coal combustion in “Toy Train”, transboundary pollutants, etc. Besides, the favorable meteorological conditions augmented the overall increase in total PM load that

may consequently lead to the formation of secondary organic aerosols (SOA) in the atmosphere through chemical/physical processes. During the winter season, although biomass burning in Punjab and Haryana and long-range transport of continental air masses were found to be the major contributor of particulates. Comparatively, a higher concentration of PM was observed in the monsoon season which may be due to more accumulation and less wash-out of pollutants.

The findings of this study will be useful in providing yearly quality assured PM_{2.5} and PM₁₀ concentrations for efficient air quality mitigation policies in the Himalayan region, as well as invalidating model results for future air quality studies. In future research, we will work on source apportionment and factor contribution of potential source regions to enhance the accuracy and scientific quality of our models.

Supplementary Information The online version contains supplementary material available at <https://doi.org/10.1007/s41810-021-00106-5>.

Acknowledgements The authors are thankful to the Director, CSIR-NPL and Head, Environmental Sciences and Biomedical Metrology Division (ES&BMD), CSIR–NPL for their encouragement and support. Authors are also thankful to Mr. Bivek Gurung and Mrs. Yashodhara Yadav, Bose Institute, Darjeeling for PM sampling and providing the relevant data-sets. Authors thankfully acknowledge the NOAA Air Resources Laboratory for download of the air mass trajectories (<http://www.arl.noaa.gov/ready/hysplit4.html>).

Author contributions Conception and design of the study were planned by SKS, RKK, TKM, AC; Data collection and analysis were performed by AR, SM, NC and AG; the first draft was written by AR and SKS. Data interpretation was carried out by AR, AC, TKM, RKK and SKS. All the authors read and approved the final manuscript.

Funding The authors are thankfully acknowledged the Department of Science and Technology, Ministry of Science and Technology (Government of India), New Delhi-110016, India for providing financial support for this study (DST/CCP/Aerosol/88/2017).

Data availability The datasets developed during the current study are available from the corresponding author on reasonable request.

Declarations

Conflict of interest The authors declare that they have no conflict of interest.

Ethical approval Not applicable.

Consent to participate Not applicable.

Consent to publish Not applicable.

References

- Aamaas B, Myhre G, Samset BH, Stjern CW (2017) The climate impacts of current black carbon and organic carbon emissions. CICERO Report
- Adak A, Chatterjee A, Singh AK, Sarkar C, Ghosh S, Raha S (2013) Atmospheric fine mode particulates at eastern Himalaya, India: role of meteorology, long-range transport, and local anthropogenic sources. *Aerosol Air Quality Res* 14(1):440–450
- Alves CA, Pio CA (2005) Secondary organic compounds in atmospheric aerosols: speciation and formation mechanisms. *J Braz Chem Soc* 16(5):1017–1029
- Apollo M (2017). The population of Himalayan regions—by the numbers: Past, present, and future. In: Efe R, Öztürk M (eds) *Contemporary studies in environment and tourism*, Scholars Publishing, Cambridge, p 145–160
- Arhami M, Shahne MZ, Hosseini V, Haghighat NR, Lai AM, Schauer JJ (2018) Seasonal trends in the composition and sources of PM_{2.5} and carbonaceous aerosol in Tehran. *Iran Environ Pollution* 239:69–81
- Babu S, Mohapatra KP, Das A, Yadav GS, Singh R, Chandra P, Avasthe RK, Kumar A, Devi MT, Singh VK, Panwar AS (2021) Integrated farming systems: climate-resilient sustainable food production system in the Indian Himalayan region. In: *Exploring synergies and trade-offs between climate change and the sustainable development goals*, Springer, Singapore, pp 119–143
- Bhattacharyya T, Chatterjee A, Das SK, Singh S, Ghosh SK (2020) Study of the fair-weather surface atmospheric electric field at high altitude station in Eastern Himalayas. *Atmosph Res* 239:104909
- Bikkina S, Sarin M (2019) Brown carbon in the continental outflow to the North Indian Ocean. *Environ Sci* 21(6):970–987
- Cajee L (2018) Physical aspects of the Darjeeling Himalaya: understanding from a geographical perspective. *IOSR J Human Soc Sci* 2(3):66–79
- Callén MS, De la Cruz MT, López JM, Mastral AM (2011) PAH in airborne particulate matter: carcinogenic character of PM₁₀ samples and assessment of the energy generation impact. *Fuel Process Technol* 92(2):176–182
- Castro LM, Pio CA, Harrison RM, Smith DJT (1999) Carbonaceous aerosol in urban and rural European atmospheres: estimation of secondary organic carbon concentrations. *Atmosph Environ* 33:2771–2781
- Chatterjee A, Adak A, Singh AK, Srivastava MK, Ghosh SK, Tiwari S, Devara PCS, Raha S (2010) Aerosol chemistry over a high-altitude station at the northeastern Himalayas, India. *Plos One* 5(6):e11122
- Chatterjee A, Dutta M, Ghosh A, Ghosh SK, Roy A (2020) Relative role of black carbon and sea-salt aerosols as cloud condensation nuclei over a high-altitude urban atmosphere in eastern Himalaya. *Sci Total Environ* 742:140468
- Chatterjee A, Mukherjee S, Dutta M, Ghosh A, Ghosh SK, Roy A (2021) High rise in carbonaceous aerosols under very low anthropogenic emissions over eastern Himalaya, India: Impact of lockdown for COVID-19 outbreak. *Atmosph Environ* 244:117947
- Chen Y, Xie S, Luo B (2018) Seasonal variations of transport pathways and potential sources of PM_{2.5} in Chengdu, China (2012–2013). *Front Environ Sci Eng* 12(1):12
- Chen CH, Wu CD, Chiang HC, Chu D, Lee KY, Lin WY, Yeh JI, Tsai KW, Guo YLL (2019) The effects of fine and coarse particulate matter on lung function among the elderly. *Sci Rep* 9(1):1–8
- Chow JC, Watson JG, Chen LWA, Arnott WP, Moosmüller H, Fung K (2004) Equivalence of elemental carbon by thermal/optical reflectance and transmittance with different temperature protocols. *Environ Sci Technol* 38(16):4414–4422

- Dimitriou K, Remoundaki E, Mantas E, Kassomenos P (2015) Spatial distribution of source areas of PM_{2.5} by concentration weighted trajectory (CWT) model applied in PM_{2.5} concentration and composition data. *Atmos Environ* 116:138–145
- Dinoi A, Cesari D, Marinoni A, Bonasoni P, Riccio A, Chianese E, Tirimberio G, Naccarato A, Sprovieri F, Andreoli V, Moretti S, Gulli D, Calidonna CR, Ammassato I, Contini D (2017) Inter-comparison of carbon content in PM_{2.5} and PM₁₀ collected at five measurement sites in southern Italy. *Atmosphere* 8(12):243
- Du Y, Xu X, Chu M, Guo Y, Wang J (2016) Air particulate matter and cardiovascular disease: the epidemiological, biomedical, and clinical evidence. *J Thorac Dis* 8(1):E8
- Dumka UC, Tiwari S, Kaskaoutis DG, Soni VK, Safai PD, Attri SD (2019) Aerosol and pollutant characteristics in Delhi during a winter research campaign. *Environ Sci Pollut Res* 26(4):3771–3794
- Falcon-Rodriguez CI, Osornio-Vargas AR, Sada-Ovalle I, Segura-Medina P (2016) Aeroparticles, composition, and lung diseases. *Front Immunol* 7:3
- Gajanananda K, Kuniyal JC, Momin GA, Rao PSP, Safai PD, Tiwari S, Ali K (2005) Trend of atmospheric aerosols over the north north-western Himalayan region, India. *Atmos Environ* 39:4817–4825
- Ghosh SK, Raha S, Abhijit C (2014) The Darjeeling facility: Cosmic rays and atmospheric sciences. *Proc Indian Natl Sci Acad-A (india)* 80:791–814
- Ghosh S, Biswas J, Guttikunda S, Roychowdhury S, Nayak M (2015) An investigation of potential regional and local source regions affecting fine particulate matter concentrations in Delhi, India. *J Air Waste Manag Assoc* 65(2):218–231
- Hanigan IC, Broome RA, Chaston TB, Cope M, Dennekamp M, Heyworth JS, Heathcote K, Horsley JA, Jalaludin B, Jegasothy E, Johnston FH, Knibbs LD, Pereira G, Vardoulakis S, Hoorn SV, Morgan GG (2021) Avoidable mortality attributable to anthropogenic fine particulate matter (PM_{2.5}) in Australia. *Int J Environ Res Public Health* 18(1):254
- Hegde P, Kawamura K (2012) Seasonal variations of water-soluble organic carbon, dicarboxylic acids, keto carboxylic acids, and α -dicarbonyls in Central Himalayan aerosols. *Atmos Chem Phys* 12(14):6645–6665
- Hegde P, Vyas BM, Aswini AR, Aryasree S, Nair PR (2020) Carbonaceous and water-soluble inorganic aerosols over a semi-arid location in northwest India: Seasonal variations and source characteristics. *J Arid Environ* 172:104018
- Hernández-Ceballos MÁ, De Felice L (2019) Air mass trajectories to estimate the “Most Likely” areas to be affected by the release of hazardous materials in the atmosphere—feasibility study. *Atmosphere* 10(5):253
- Jafar HA, Harrison RM (2020) Spatial and temporal trends in carbonaceous aerosols in the United Kingdom. *Atmospheric Pollution Research*
- Jin Y, Yan C, Sullivan AP, Liu Y, Wang X, Dong H, Chen S, Zeng L, Collett JL Jr, Zheng M (2020) Significant contribution of primary sources to water-soluble organic carbon during spring in Beijing. *China Atmosphere* 11(4):395
- Joshi H, Naja M, Gupta T (2020) In-situ Measurements of aerosols from the high-altitude location in the central Himalayas. In: Measurement, analysis and remediation of environmental pollutants, Springer, Singapore, pp 59–89
- Kim HJ, Choi MG, Park MK, Seo YR (2017) Predictive and prognostic biomarkers of respiratory diseases due to particulate matter exposure. *J Cancer Prevention* 22(1):6
- Kirillova EN, Andersson A, Sheesley RJ, Kruså M, Praveen PS, Budhavant K, Safai PD, Rao PSP, Gustafsson Ö (2013) ¹³C- and ¹⁴C-based study of sources and atmospheric processing of water-soluble organic carbon (WSOC) in South Asian aerosols. *J Geophys Res* 118(2):614–626
- Kontuľ I, Kaizer J, Jeřkovský M, Steier P, Povinec PP (2020) Radio-carbon analysis of carbonaceous aerosols in Bratislava, Slovakia. *J Environ Radioact* 218:106221
- Kumar A, Attri AK (2015) Biomass combustion a dominant source of carbonaceous aerosols in the ambient environment of the Western Himalayas. *Aerosol Air Quality Res* 16(3):519–529
- Lamsal P, Kumar L, Shabani F, Atreya K (2017) The greening of the Himalayas and Tibetan Plateau under climate change. *Global Planet Change* 159:77–92
- Li C, Yan F, Kang S, Yan C, Hu Z, Chen P, Gao S, Zhang C, He C, Kaspari S, Stubbins A (2020a) Carbonaceous matter in the atmosphere and glaciers of the Himalayas and the Tibetan plateau: an investigative review. *Environ Int* 146:106281
- Li Y, Zhao W, Fu J, Liu Z, Li C, Zhang J, He C, Wang K (2020b) Joint governance regions and major prevention periods of PM_{2.5} pollution in china based on wavelet analysis and concentration-weighted trajectory. *Sustain* 12(5):2019
- Loomis D, Grosse Y, Lauby-Secretan B, El Ghissassi F, Bouvard V, Benbrahim-Tallaa L, Guha N, Baan R, Mattock H, Straif K (2013) The carcinogenicity of outdoor air pollution. *Lancet Oncol* 14(13):1262
- Mahapatra PS, Sinha PR, Boopathy R, Das T, Mohanty S, Sahu SC, Gurjar BR (2018) Seasonal progression of atmospheric particulate matter over an urban coastal region in peninsular India: role of local meteorology and long-range transport. *Atmos Res* 199:145–158
- Markou MT, Kassomenos P (2010) Cluster analysis of 5 years of back trajectories arriving in Athens. *Greece Atmos Res* 98(2–4):438–457
- Masiol M, Hopke PK, Felton HD, Frank BP, Rattigan OV, Wurth MJ, LaDuke GH (2017) Analysis of major air pollutants and submicron particles in New York City and Long Island. *Atmos Environ* 148:203–214
- NESCAUM (2002) Trajectory analysis of potential source regions affecting class I areas in the MANE-VU region. Northeast States for Coordinated Air-Use Management, Boston, MA
- Ojha N, Sharma A, Kumar M, Girach I, Ansari TU, Sharma SK, Singh N, Pozzer A, Gunthe SS (2020) On the widespread enhancement in fine particulate matter across the Indo-Gangetic Plain towards winter. *Sci Rep* 10(1):1–9
- Panicker AS, Kumar VA, Raju MP, Pandithurai G, Safai PD, Beig G, Das S (2021) CCN activation of carbonaceous aerosols from different combustion emissions sources: a laboratory study. *Atmos Res* 248:105252
- Pant P, Harrison RM (2012) Critical review of receptor modelling for particulate matter: a case study of India. *Atmos Environ* 49:1–12
- Peters A (2005) Particulate matter and heart disease: evidence from epidemiological studies. *Toxicol Appl Pharmacol* 207(2):477–482
- Pintér M, Utry N, Ajtai T, Kiss-Albert G, Jancsek-Turóczi B, Imre K, Palágyi A, Manczinger L, Vágvölgyi C, Horváth E, Kováts N, Gelencsér A, Szabó G, Bozóki Z (2017) Optical properties, chemical composition, and the toxicological potential of urban particulate matter. *Aerosol and Air Quality Research* 17(6):1515–1526
- Pope CA III, Dockery DW (2006) Health effects of fine particulate air pollution: lines that connect. *J Air Waste Manag Assoc* 56(6):709–742
- Rai A, Mukherjee S, Chatterjee A, Choudhary N, Kotnala G, Mandal TK, Sharma SK (2020) Seasonal variation of OC, EC, and WSOC of PM₁₀ and Their CWT analysis over the Eastern Himalaya. *Aerosol Sci Eng* 4(1):26–40
- Rajput P, Sarin M, Kundu SS (2013) Atmospheric particulate matter (PM_{2.5}), EC, OC, WSOC, and PAHs from NE-Himalaya: abundances and chemical characteristics. *Atmos Pollut Res* 4(2):214–221

- Ram K, Sarin MM (2010) Spatio-temporal variability in atmospheric abundances of EC, OC, and WSOC over Northern India. *J Aerosol Sci* 41(1):88–98
- Ram K, Sarin MM, Tripathi SN (2012) Temporal trends in atmospheric $PM_{2.5}$, PM_{10} , elemental carbon, organic carbon, water-soluble organic carbon, and optical properties: impact of biomass burning emissions in the Indo-Gangetic Plain. *Environ Sci Technol* 46(2):686–695
- Ram K, Bhattarai H, Cong Z (2020) Chemical components and distributions of aerosols in the third pole. In: *Water quality in the third pole*. Elsevier, pp 43–67
- Ramachandran S, Rupakheti M (2021) Inter-annual and seasonal variations in optical and physical characteristics of columnar aerosols over the Pokhara Valley in the Himalayan foothills. *Atmos Res* 248:105254
- Ramachandran S, Rupakheti M, Lawrence MG (2020) Aerosol-induced atmospheric heating rate decreases over South and East Asia as a result of changing content and composition. *Sci Rep* 10(1):1–17
- Roy A, Chatterjee A, Tiwari S, Sarkar C, Das SK, Ghosh SK, Raha S (2016) Precipitation chemistry over urban, rural, and high-altitude Himalayan stations in eastern India. *Atmos Res* 181:44–53
- Saikawa E, Panday A, Kang S, Gautam R, Zusman E, Cong ZSES, Adhikary B (2019). Air pollution in the hindu kush Himalaya. In: Wester P, Mishra A, Mukherji A, Shrestha AB (eds) *The hindu kush Himalaya assessment—mountains, climate change, sustainability and people*. Springer Nature Switzerland AG, Cham, pp 339–387
- Sarkar C, Chatterjee A, Singh AK, Ghosh SK, Raha S (2015) Characterization of black carbon aerosols over darjeeling—a high altitude himalayan station in eastern India. *Aerosol Air Qual Res* 15:465–478
- Sarkar C, Roy A, Chatterjee A, Ghosh SK, Raha S (2019) Factors controlling the long-term (2009–2015) trend of $PM_{2.5}$ and black carbon aerosols at eastern Himalaya. *India Sci Total Environ* 656:280–296
- Sen A, Karapurkar SG, Saxena M, Shenoy DM, Chatterjee A, Choudhuri AK, Das T, Khan AH, Kuniyal JC, Pal S, Singh DP, Sharma SK, Kotnala RK, Mandal TK (2018) Stable carbon and nitrogen isotopic composition of PM_{10} over Indo-Gangetic Plains (IGP), adjoining regions, and Indo-Himalayan Range (IHR) during a winter 2014 campaign. *Environ Sci Pollut Res* 25(26):26279–26296
- Sharma SK, Mandal TK, Sharma C, Kuniyal JC, Joshi R, Dhyani PP, Rohtash, Ghayas H, Gupta NC, Sharma P, Saxena M, Sharma A, Arya BC, Kumar A (2014) Measurements of particulate ($PM_{2.5}$), BC, and trace gases over the north-western Himalayan region of India. *MAPAN* 29(4):243–253
- Sharma SK, Mandal TK, Shenoy DM, Bardhan P, Srivastava MK, Chatterjee A, Saxena M, Saraswati SBP, Ghosh SK (2015) Variation of stable carbon and nitrogen isotopes composition of PM_{10} over Indo Gangetic Plain of India. *Bull Environ Contam Toxicol* 95(5):661–669
- Sharma SK, Agarwal P, Mandal TK, Karapurkar SG, Shenoy DM, Peshin SK et al (2017) Study on ambient air quality of megacity Delhi, India during odd-even Strategy. *MAPAN* 32(2):155–165
- Sharma SK, Mandal TK, Dey AK, Deb N, Jain S, Saxena M, Pal S, Choudhuri AK, Yadav S (2018) Carbonaceous and inorganic species in PM_{10} during wintertime over Giridih, Jharkhand (India). *J Atmos Chem* 75:219–233
- Sharma SK, Choudhary N, Kotnala G, Das D, Mukherjee S, Ghosh A, Vijayan N, Rai A, Chatterjee A, Mandal TK (2020). Winter-time carbonaceous species and trace metals in PM_{10} in Darjeeling: a high altitude town in the eastern Himalayas. *Urban Climate* 34:100668
- Sharma SK, Mukherjee S, Choudhary N, Rai A, Ghosh A, Chatterjee A, Vijayan N, Mandal TK (2021) Seasonal variation and sources of carbonaceous species and elements in $PM_{2.5}$ and PM_{10} over the Eastern Himalaya. *Environ Sci Pollut Res Int*. <https://doi.org/10.1007/s11356-021-14361-z>.
- Silva RA, West JJ, Lamarque JF, Shindell DT, Collins WJ, Dalsoren S, Faluvegi G, Folberth G, Horowitz LW, Nagashima T, Naik V, Rumbold ST, Sudo K, Takemura T, Bergmann D, Smith PC, Cionni I, Doherty RM, Eyring V, Josse B, MacKenzie IA, Plummer D, Righi M, Stevenson DS, Strode S, Szopa S, Zeng, G. (2016) The effect of future ambient air pollution on human premature mortality to 2100 using output from the ACCMIP model ensemble. *Atmos Chem Phys* 16(15):9847
- Srinivas B, Sarin MM (2014) $PM_{2.5}$, EC, and OC in an atmospheric outflow from the Indo-Gangetic Plain: temporal variability and aerosol organic carbon-to-organic mass conversion factor. *Sci Total Environ* 487:196–205
- Srivastava P, Naja M (2020) Characteristics of carbonaceous aerosols derived from long-term high-resolution measurements at a high-altitude site in the central Himalayas: radiative forcing estimates and role of meteorology and biomass burning. *Environ Sci Pollut Res* 1–17
- Su L, Yuan Z, Fung JC, Lau AK (2015) A comparison of HYSPLIT backward trajectories generated from two GDAS datasets. *Sci Total Environ* 506:527–537
- Suzuki Y, Matsunaga K, Yamashita Y (2020) Assignment of $PM_{2.5}$ sources in western Japan by non-negative matrix factorization of concentration-weighted trajectories of GED-ICP-MS/MS element concentrations. *Environ Pollut* 270:116054
- Tiwari S, Dumka UC, Gautam AS, Kaskaoutis DG, Srivastava AK, Bisht DS, Chakrabarty RK, Sumlin BJ, Solomon F (2017) Assessment of $PM_{2.5}$ and PM_{10} over Guwahati in Brahmaputra River Valley: Temporal evolution, source apportionment, and meteorological dependence. *Atmos Pollut Res* 8(1):13–28
- Tripathee L, Kang S, Chen P, Bhattarai H, Guo J, Shrestha KL, Sharma CM, Ghimire PS, Huang J (2021) Water-soluble organic and inorganic nitrogen in ambient aerosols over the Himalayan middle hills: Seasonality, sources, and transport pathways. *Atmos Res* 250:105376
- Tse-ring K, Sharma E, Chettri N, Shrestha AB (2010) Climate change vulnerability of mountain ecosystems in the Eastern Himalayas—Synthesis Report. International Centre for Integrated Mountain Development (ICIMOD), Kathmandu, Nepal
- Wang YQ, Zhang XY, Draxler RR (2009) TrajStat: GIS-based software that uses various trajectory statistical analysis methods to identify potential sources from long-term air pollution measurement data. *Environ Model Softw* 24(8):938–939
- Wei N, Ma C, Liu J, Wang G, Liu W, Zhuoga D, Xiao D, Yao J (2019) Size-segregated characteristics of carbonaceous aerosols during the monsoon and non-monsoon seasons in Lhasa in the Tibetan Plateau. *Atmosphere* 10(3):157
- World Health Organization, Regional Office for Europe & Joint (2006) Health risks of particulate matter from long-range transboundary air pollution (No. EUR/05/5046028). WHO Regional Office for Europe, Copenhagen
- WHO (2016) Ambient air pollution: A global assessment of exposure and burden of disease
- Xin Y, Wang G, Chen L (2016) Identification of long-range transport pathways and potential sources of PM_{10} in the Tibetan Plateau uplift area: Case study of Xining, China, in 2014. *Aerosol Air Quality Research* 16(4):1044–1054
- Xu Z, Wen T, Li X, Wang J, Wang Y (2015) Characteristics of carbonaceous aerosols in Beijing based on two-year observation. *Atmos Pollut Res* 6(2):202–208
- Yang W, Wang G, Bi C (2017) Analysis of long-range transport effects on $PM_{2.5}$ during a short severe haze in Beijing. *China Aerosol Air Qual Res* 17:1610–1622
- Yang W, Xie S, Zhang Z, Hu J, Zhang L, Lei X, Zhong L, Hao Y, Shi F (2019) Characteristics and sources of carbonaceous aerosol across

- urban and rural sites in a rapidly urbanized but low-level industrialized city in the Sichuan Basin. *China Environ Sci Pollution Res* 26(26):26646–26663
- Yu GH, Cho SY, Bae MS, Park SS (2014) Difference in production routes of water-soluble organic carbon in $PM_{2.5}$ observed during non-biomass and biomass burning periods in Gwangju, Korea. *Environ Sci* 16(7):1726–1736
- Yuan Q, Xu J, Liu L, Zhang A, Liu Y, Zhang J, Wan X, Li M, Qin K, Cong Z, Wang Y, Kang S, Shi Z, Pósfai M, Li W (2020a) Evidence for Large Amounts of Brown Carbonaceous Tarballs in the Himalayan Atmosphere. *Environ Sci Technology Letters*
- Yuan Q, Wan X, Cong Z, Li M, Liu L, Shu S, Liu R, Xu L, Zhang J, Ding X, Li W (2020b) In situ observations of light-absorbing carbonaceous aerosols at himalaya: analysis of the south asian sources and trans-himalayan valleys transport pathways. *J Geophys Res* 125(18):e2020JD032615
- Zhang Q, Worsnop DR, Canangaratna MR, Jimenez JL (2005) Hydrocarbon-like and oxygenated organic aerosols in Pittsburgh: Insights into sources and processes of organic aerosol. *Atmos Chem Phys* 5:3289–3311
- Zhang J, Tong L, Huang Z, Zhang H, He M, Dai X, Zheng J, Xiao H (2018) Seasonal variation and size distributions of water-soluble inorganic ions and carbonaceous aerosols at a coastal site in Ningbo, China. *Sci Total Environ* 639:793–803
- Zhang X, Li Z, Wang F, Song M, Zhou X, Ming J (2020) Carbonaceous Aerosols in PM_1 , $PM_{2.5}$, and PM_{10} Size Fractions over the Lanzhou City, Northwest China. *Atmos* 11(12):1368
- Zhu L, Zhang Y, Kan X, Wang J (2018) Transport paths and identification for potential sources of haze pollution in the yangtze river delta urban agglomeration from 2014 to 2017. *Atmosphere* 9(12):502
- Zhu JJ, Chen YC, Shie RH, Liu ZS, Hsu CY (2020) Predicting carbonaceous aerosols and identifying their source contribution with advanced approaches. *Chemosphere* 128966